Manuscript # ACP-2015-793

Responses to the Reviewer

After adding the new Table 3, Figure 12 and the related text, the revised manuscript presents a clearer picture about the mechanism that leads to the accumulation of nitrate in the UTLS over TP/SASM. It is, however, not clear enough. I am not questioning your conclusion about the importance of upward transport and the gas–to–aerosol conversion of HNO3, but I want to know the source of HNO3 that is converted to aerosol nitrate. You calculated the net–chemical production of HNO3 by subtracting the losses in reactions R24–R25 from the total production of HNO3 in reactions R1–R23. In the range 100–400 hPa, the calculated net–chemical production looks much smaller than the production of nitrate from gas–to–aerosol conversion (Fig. 12). Moreover, you did not included the loss of HNO3 in reaction with NH3 in your calculation of the net–chemical production of HNO3. If the HNO3+NH3 reaction is included, as required for a chemical budget, the net–chemical production of HNO3 should be even much smaller than shown in Fig. 12, and negative around 200–300 hPa. So, what is the origin of HNO3 converted to nitrate? From transport of air masses outside the range 100–400 hPa? If so, you are suggested to plot this source on Fig. 12. In addition, I suggest to display the vertical profile of the mixing ratio of HNO3 on Fig. 12 and discuss the major chemical sources of HNO3 and their vertical distributions.

Response:

Following the suggestion, Fig. 12 is revised in the manuscript to show the vertical profiles of transport contribution of HNO_3 and the HNO_3 mixing ratio. The following discussions have been added in Sec. 6.2:

Figure 12 shows the net chemical production of HNO_3 by gas-phase reactions and heterogeneous reactions (chemical production by reactions R1-R23 minus chemical loss by reactions R24-R25 in Table 3) summed over the TP/SASM region. The net chemical production has an overall trend of decreasing with altitude. Since NO_x emissions from aircraft and lightning are located between 200–300 hPa over the TP/SASM region during summer (Martin et al., 2007; Murray et al., 2012; Pitari et al., 2015), net chemical production of HNO_3 shows a small peak at those altitudes. The mixing ratio of HNO_3 decreases with altitude between 500 and 200 hPa and increases with altitude above 200 hPa. At 100 hPa, the average HNO_3 mixing ratio over the TP/SASM region agrees with the values of 300–400 pptv over the same region shown in Fig. 4.

Figure 12 also shows the transport of HNO_3 over the TP/SASM region, defined as convergence of horizontal flux of HNO_3 (inflow minus outflow) plus convergence of vertical flux of HNO_3 (inflow minus outflow) for a specific vertical model layer. At altitudes below 200 hPa, concentrations of HNO_3 over the TP/SASM region are dependent on the net chemical production by gas-phase reactions and heterogeneous reactions as well as the transport of HNO_3.The vertical variation of the horizontal transport (the north-south and the east-west transport) follows the development of the anticyclone in the upper troposphere during summertime. As displayed in Figs. A(a)-A(d) (see below), as the altitude increases, the westerlies enhance over the TP and the easterlies develop over the SASM region (see Fig. 1 for our definitions of TP

and SASM regions). At latitudes between 100–500 hPa, vertical transport of HNO_3 occurs over the TP due to the deep convection activities over the region which can arrive at 100–200 hPa (Fig. 11; Fadnavis et al.,2013; Qie et al., 2014).

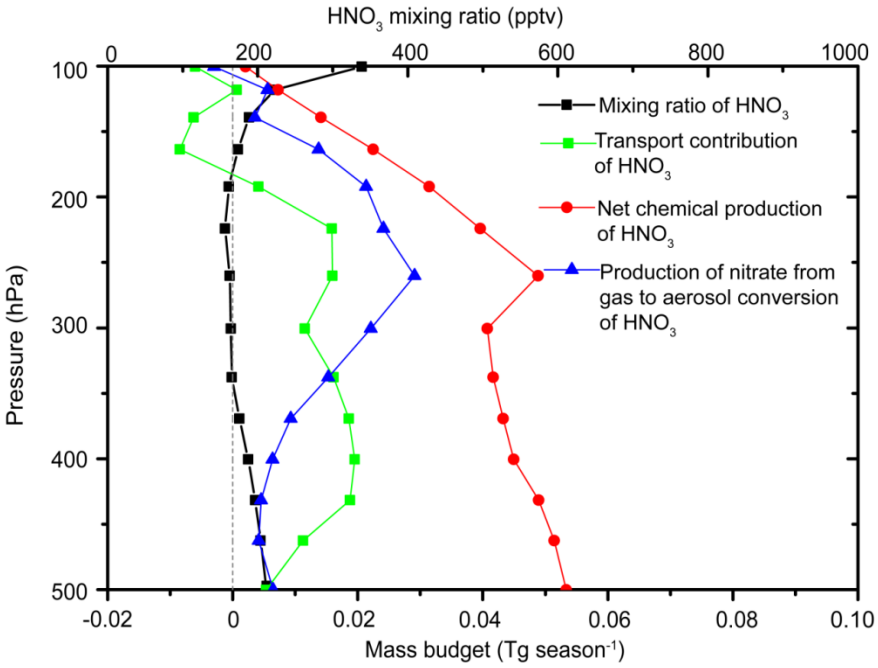

Figure 12. Profiles of the net chemical production of HNO_3 by gas-phase reactions and heterogeneous reactions (red dotted line), the production of nitrate from gas to aerosol conversion of HNO_3 (blue dotted line) and the transport contributions of HNO_3 over the TP/SASM (70–105°E, 10–40°N). Also shown is the average HNO_3 mixing ratios (black dotted line) over the TP/SASM region during summertime of year 2005.

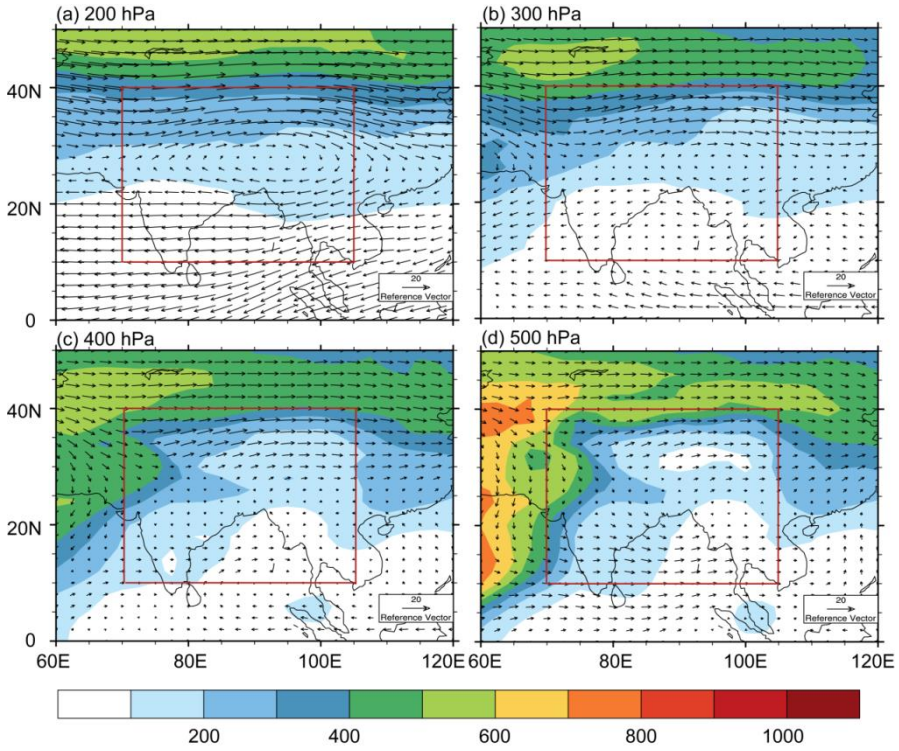

Figure A. Simulated horizontal distributions of HNO_3 mixing ratio (pptv) and horizontal wind fields from the assimilated GEOS-5 meteorological data at (a) 200 hPa, (b) 300 hPa, (c) 400 hPa, and (d) 500 hPa during summertime of year 2005. The red lines mark the TP/SASM region (70–105°E, 10–40°N).

Other points:

Figures 4 and 5: the performance of GEOS-Chem model seems to be bad in high latitudes (40–50N). Please explain this.

Response:

The comparisons between the model simulations and MLS observations in high altitudes are not as good as those in the tropical and subtropical regions due to the following reasons:

(1) NO_x emissions in high latitudes (40–50°N) have uncertainties. For example, Huang et al. (2014) reported that NO_x emissions in Russia in our simulation (taken from Emissions Database for Global Atmospheric Research, EDGAR v4.2) were underestimated by 70% compared to the Russian federal emission inventory.

(2) The 200–100 hPa altitudes in high latitudes (40–50°N) partly belong to the stratospheric grid cells (Fig. 11). For the stratospheric species, the GEOS-Chem model uses the monthly mean production rates and loss frequencies from NASA Global Modeling Initiative (GMI) Combo simulations (Duncan et al., 2007; Considine et al., 2008; Murray et al., 2012). The archived three-dimensional monthly mean production rates and loss frequencies in the stratosphere are the averages over years of 2004–2010. Although we use the emissions and meteorological fields of year 2005 in our simulation, we would consider that the tropospheric simulation can be representative of year 2005 but stratosphere simulation should represent a multi-year average. The multi-year average stratospheric conditions might not capture well the characteristics of year 2005

concentrations from MLS.

(3) As discussed in Livesey et al. (2011), although MLS datasets in the UTLS are considered to be valuable in evaluating model results, the uncertainties of MLS datasets between 215–100 hPa are relatively larger than those in the stratosphere (100–6.8 hPa).

Figure 7: while I can see the high value zones of nitrate, ammonium, OC, BC, and PM2.5 in the UTLS over TP/SASM, I can hardly see that of sulfate. Fadnavis et al. (2013) reported a very clear high value zone of sulfate in their Fig. 1 (c). Why is there such a large difference? What could be the problem in your or their simulations?

Response:

The performance of ECHAM5-HAMMOZ in simulating sulfate has been examined in previous studies by comparing the model results with observations (Stier et al., 2005; Pozzoli et al., 2008a, b; Pozzoli et al., 2011). Overall, the ECHAM5-HAMMOZ overestimated sulfate concentrations in North America and Europe by about a factor of 2 (Stier et al., 2005). For Aisa and in the low latitude regions, limited comparisions were conducted. Pozzoli et al. (2008a) compared simulated sulfate concentrations from the ECHAM5-HAMMOZ model with flight measurements from the Transport and Chemical Evolution over the Pacific (TRACE-P) campaign in March–April 2001. They showed that the ECHAM5-HAMMOZ overestimated sulfate concentrations for the low latitudes (10–25°N, 110–150°E) with a mean absolute bias of 110%. Such overestimation of sulfate in the lower troposphere could lead to an overestimation of sulfate transported upward to the UTLS over the TP/SASM region in summer, which could explain in part that the high value zone of sulfate is more obvious in Fadnavis et al. (2013).

The simulated sulfate in ECHAM5-HAMMOZ also accounted for the formation of sulfate aerosol on mineral dust particles (Pozzoli et al., 2008a), whereas this mechanism is not included in the standard version of GEOS-Chem. Since the concentrations of mineral dust show high value zone over the anticyclone region during summertime (as discussed in our Sec. 5 and Fadnavis et al. (2013)), sulfate formation on dust might result in a more obvious high value zone of sulfate in Fadnavis et al. (2013).

In addition, the advection and convection schemes in the two models are different, which might have contributed to the differences in transport and distribution of pollutants.

Figure 9: you show in Fig. 7(c) two high PM2.5 zones, but there is only one zone of high aerosol extinction coefficient in Fig. 9(a). Why?

Response:

We have described in the text that $PM_{2.5}$ in Fig.7 is the sum of anthropogenic aerosol species (defined as the sum of sulfate, nitrate, ammonium, BC, and OC). Following the suggestions of previous reviewers, aerosol extinction coefficient in Fig. 9 is calculated with the contributions of both anthropogenic and natural aerosols. The natural aerosols include sea salt (sum of mass over two size bins of 0.1–0.5, 0.5–8 μm) and mineral dust (sum of mass over four size bins of 0.1–1.0, 1.0–1.8, 1.8–3.0, 3.0–6.0 μm). We have now clarified the consideration of aerosol species in the captions of Figs. 7 and 9.

Lines 705–713: they are many many percent values in Table 4, but the percent values you mention here are actually not shown in Table 4. Please give values, from which you calculated the percent values, e.g., “46.8% (from 0.94 μg m^{-3} to 0.50 μg m^{-3})”.

Response:

Thanks for the suggestions. We have revised the descriptions as follows:” As shown in Table 4, for the surface layer, simulated nitrate concentration over the TP/SASM region decreases by 46.8% (from 0.94 μg m^{-3} to 0.50 μg m^{-3}) with a 50% reduction in anthropogenic NO_x emissions in Asia, and it decreases by 22.3% (from 0.94 μg m^{-3} to 0.73 μg m^{-3}) when anthropogenic NH_3 emissions are reduced by the same percentage, indicating that surface-layer nitrate aerosol is more sensitive to anthropogenic emissions of NO_x than to those of NH_3. Relative to the baseline simulation, simulated nitrate concentrations at 200 hPa and 100 hPa decrease, respectively, by 49.0% (from 7.57×10^{-2} μg m^{-3} to 3.86×10^{-2} μg m^{-3}) and 17.7% (from 6.90×10^{-2} μg m^{-3} to 5.68×10^{-2} μg m^{-3}) with a 50% reduction in NH_3 emissions, whereas only by 2.1% (from 7.57×10^{-2} μg m^{-3} to 7.41×10^{-2} μg m^{-3}) and 1.3% (from 6.90×10^{-2} μg m^{-3} to 6.81×10^{-2} μg m^{-3}) with a 50% reduction in NO_x emissions.”

Reference

Considine, D. B., Logan, J. A., and Olsen, M. A.: Evaluation of near-tropopause ozone distributions in the Global Modeling Initiative combined stratosphere/troposphere model with ozonesonde data, Atmos. Chem. Phys., 8, 2365–2385, 2008.

Duncan, B., Strahan, S., Yoshida, Y., Steenrod, S., and Livesey, N.: Model study of the cross-tropopause transport of biomass burning pollution, Atmos. Chem. Phys., 7, 3713–3736, 2007.

Fadnavis, S., Semeniuk, K., Pozzoli, L., Schultz, M., Ghude, S., Das, S., and Kakatkar, R.: Transport of aerosols into the UTLS and their impact on the Asian monsoon region as seen in a global model simulation, Atmos. Chem. Phys., 13, 8771–8786, 2013.

Huang, K., Fu, J. S., Hodson, E. L., Dong, X., Cresko, J., Prikhodko, V. Y., Storey, J. M., and Cheng, M.-D.: Identification of missing anthropogenic emission sources in Russia: Implication for modeling arctic haze, Aerosol and Air Quality Reasearch, 14, 1799–1811, 2014.

Livesey, N. J., Read, W. G., Wagner, P. A., Froidevaux, L., Lambert, A., Manney, G. L., Pumphrey, H. C., Santee, M. L., Schwartz, M. J., Wang, S., Cofield, R. E., Cuddy, D. T., Fuller, R. A., Jarnot, R. F., Jiang, J. H., and Knosp, B. W.: Version 3.3 Level 2 data quality and description document, JPL D-33509, 2011.

Martin, R. V., Sauvage, B., Folkins, I., Sioris, C. E., Boone, C., Bernath, P., and Ziemke, J.: Space-based constraints on the production of nitric oxide by lightning, J. Geophys. Res., 112, D09309, doi:10.1029/2006JD007831, 2007.

Murray, L. T., Jacob, D. J., Logan, J. A., Hudman, R. C., and Koshak, W. J.: Optimized regional and interannual variability of lightning in a global chemical transport model constrained by LIS/OTD satellite data, J. Geophys. Res., 117, D20307, doi:10.1029/2012JD017934, 2012.

Pitari, G., Iachetti, D., Genova, G. D., De Luca, N., Søvde, O., Hodnebrog, Ø., Lee, D. S., and Lim, L. L.: Impact of coupled NO_x/aerosol aircraft emissions on ozone photochemistry and radiative forcing, Atmosphere,6, 751–782, doi:10.3390/atmos6060751, 2015.

Pozzoli, L., Bey, I., Rast, J. S., Schultz, M. G., Stier, P., and Feichter, J.: Trace gas and aerosol interactions in the fully coupled model of aerosol-chemistry-climate ECHAM5- HAMMOZ: 1. Model description and insights from the spring 2001 TRACE-P experiment, J. Geophys. Res., 113, D07308, doi:10.1029/2007JD009007, 2008a.

Pozzoli, L., Bey, I., Rast, J. S., Schultz, M. G., Stier, P., and Feichter, J.: Trace gas and aerosol interactions in the fully coupled model of aerosol-chemistry-climate ECHAM5- HAMMOZ: 2. Impact of heterogeneous chemistry on the global aerosol distributions, J. Geophys. Res., 113, D07309, doi:10.1029/2007JD009008, 2008b.

Pozzoli, L., Janssens-Maenhout, G., Diehl, T., Bey, I., Schultz, M. G., Feichter, J., Vignati, E., and Dentener, F.: Re-analysis of tropospheric sulfate aerosol and ozone for the period 1980–2005 using the aerosol-chemistry-climate model ECHAM5-HAMMOZ, Atmos. Chem. Phys., 11, 9563–9594, doi:10.5194/acp-11-9563-2011, 2011.

Qie, X., Wu, X., Yuan, T., Bian, J., and Lü, D.: Comprehensive Pattern of Deep Convective Systems over the Tibetan Plateau–South Asian Monsoon Region Based on TRMM Data, J. Clim., 27, 6612–6626, 2014.

Stier, P., Feichter, J., Kinne, S., Kloster, S., Vignati, E., Wilson, J., Ganzeveld, L., Tegen, I., Werner, M., Balkanski, Y., Schulz, M., Boucher, O., Minikin, A., and Petzold, A.: The aerosol-climate model ECHAM5-HAM, Atmos. Chem. Phys., 5, 1125–1156, doi:10.5194/acp-5-1125-2005, 2005.

Summertime nitrate aerosol in the upper troposphere and lower stratosphere over the Tibetan Plateau and the South Asian summer monsoon region

Yixuan Gu[a,b], Hong Liao[c,*], and Jianchun Bian[d]

[a]State Key Laboratory of Atmospheric Boundary Layer Physics and Atmospheric Chemistry (LAPC), Institute of Atmospheric Physics, Chinese Academy of Sciences, Beijing, China.

[b]University of Chinese Academy of Sciences, Beijing, China

[c]School of Environmental Science and Engineering, Nanjing University of Information Science & Technology, Nanjing, China

[d]Key Laboratory of Middle Atmosphere and Global Environment Observation (LAGEO), Institute of Atmospheric Physics, Chinese Academy of Sciences, Beijing, China.

*Corresponding author address:

Prof. Hong Liao

School of Environmental Science and Engineering

Nanjing University of Information Science & Technology

Nanjing 210044, China

E-mail: hongliao@nuist.edu.cn

Abstract

We use the global three-dimensional Goddard Earth Observing System chemical transport model (GEOS-Chem) to examine the contribution of nitrate aerosol to aerosol concentrations in the upper troposphere and lower stratosphere (UTLS) over the Tibetan Plateau and the South Asian summer monsoon (TP/SASM) region during summertime of year 2005. Simulated surface-layer aerosol concentrations are compared with ground-based observations, and simulated aerosols in the UTLS are evaluated by using the Stratospheric Aerosol and Gas Experiment II satellite data. Simulations show elevated aerosol concentrations of sulfate, nitrate, ammonium, black carbon, organic carbon, and $PM_{2.5}$ (particles with diameter equal or less than 2.5 μm, defined as the sum of sulfate, nitrate, ammonium, black carbon, and organic carbon aerosols in this study) in the UTLS over the TP/SASM region throughout the summer. Nitrate aerosol is simulated to be of secondary importance near the surface but the most dominant aerosol species in the UTLS over the studied region. Averaged over summertime and over the TP/SASM region, C_{NIT} (the ratio of nitrate concentration to $PM_{2.5}$ concentration) values are 5–35% at the surface, 25–50% at 200 hPa, and could exceed 60% at 100 hPa. The mechanisms for the accumulation of nitrate in the UTLS over the TP/SASM region include vertical transport and the gas-to-aerosol conversion of HNO_3 to form nitrate. The high relative humidity and low temperature associated with the deep convection over the TP/SASM region are favorable for the gas-to-aerosol conversion of HNO_3.

1 Introduction

Aerosols in the upper troposphere and lower stratosphere (UTLS) have much longer residence times than those in the lower troposphere, influencing atmospheric chemistry and the Earth's climate with large spatial and temporal coverage (Rasch et al., 2008). Aerosols in the UTLS influence the concentrations of chemical species via changes in photolysis rates and heterogeneous reactions (Pitari et al., 2014). For example, heterogeneous reactions on sulfate aerosol can perturb the chemical partitioning in the lower stratosphere, leading to significant O_3 depletion through enhanced chlorine, bromine, and odd-hydrogen catalytic cycle (Zhao et al., 1997; Considine et al., 2001; Talukdar et al., 2012; Tang et al., 2014; Pitari et al., 2014). Aerosols in the UTLS also influence climate by altering properties of cirrus clouds via homogeneous or heterogeneous ice nucleation (Li et al., 2005; Liu et al., 2009; Yin et al., 2012; Fadnavis et al., 2013). Injection of aerosols into the UTLS has been reported to induce complex responses in circulation, temperature, and water vapor (Liu et al., 2009; Wu et al., 2011; Su et al., 2011; Fadnavis et al., 2013).

Aerosols over the Tibetan Plateau (TP) and the Asian summer monsoon region are especially important. The TP is surrounded by countries with large anthropogenic emissions (Li et al., 2005; Lau et al., 2006). Aerosols from India, Southeast Asia, and southern China can be transported to the TP by prevailing winds in the premonsoon and monsoon seasons (Lawrence and Lelieveld, 2010; Xia et al., 2011). Observational and modeling studies have shown that persistent maxima of atmospheric constituents, such as water vapor (Gettelman et al., 2004; Randel and Park, 2006; Park et al., 2007), CO (Kar et

al., 2004; Li et al., 2005; Park et al., 2007, 2008, 2009), CH_4 (M. Park et al., 2004; Xiong et al., 2009), NO_x (M. Park et al., 2004), HCN (Park et al., 2008; Randel et al., 2010), C_2H_6 and C_2H_2 (Park et al., 2008), exist in the UTLS above the TP and the South Asian summer monsoon (SASM) region because of the deep convection during boreal summer. Satellite observations suggested that the convection associated with the SASM is a vital pathway to transport air mass from the lower troposphere into the stratosphere (Chen et al., 2006; Randel and Park, 2006; Randel et al., 2010; Bian et al., 2011a). The heating associated with the persistent deep convection during summertime leads to the formation of the Tibetan anticyclone in the UTLS, which acts to isolate air within the anticyclone and traps the uplifted pollutants at that altitude (Park et al., 2007; Vernier et al., 2011; Bourgeois et al., 2012; Fadnavis et al., 2013; He et al., 2014). The stratosphere-troposphere exchange (STE) over the TP contributes largely to the global STE (Chen et al., 2006).

Previous studies have reported that aerosols exist in the UTLS over the TP/SASM region. Kim et al. (2003) carried out optical measurements with a ground-based lidar in Lhasa from August to October of 1999, and found an enhancement in aerosol concentration near the local tropopause with scattering ratio (SR, the ratio of aerosol plus molecular backscatter to molecular backscatter alone) of 1.1–1.2. Tobo et al. (2007) reported an enhancement of sub-micron aerosols (effective radius r = 0.15–0.6 μm) near the summertime tropopause (about 130 to 70 hPa), on the basis of in situ balloon measurements from an Optical Particle Counter at the same location in August of 1999. Vernier et al. (2009) examined satellite measurements from the Cloud-Aerosol Lidar with Orthogonal Polarization (CALIOP) onboard

Cloud-Aerosol Lidar and Infrared Pathfinder Satellite Observation (CALIPSO) and reported the presence of small depolarizing particles with high SR values (about 1.20 at 532 nm) at 16–17 km altitude over South Asia in July and August of 2007 and 2008. Bourgeois et al. (2012) found that an aerosol layer existed at 16–18 km altitude over the Asian continent and Indian Ocean (20°S–30°N, 5–105°E) on the basis of the CALIOP observations. Recently, He et al. (2014) examined the vertical profiles of aerosol extinction coefficients measured with a Micro Pulse Lidar at Naqu, a meteorological station located in the central part of the TP, and also showed a maximum in aerosol extinction coefficient (~2.10^{-3} km^{-1}) in the UTLS (18–19 km) during the summer of 2011.

A number of previous studies have attempted to understand the chemical composition of aerosols in the UTLS. Froyd et al. (2009) measured aerosol composition with the National Oceanic and Atmospheric Administration (NOAA) single-particle mass spectrometer aboard the National Aeronautics and Space Administration (NASA) WB-57 high altitude aircraft platform, and reported that particles in the tropical tropopause layer were rich in nitrogen. Vernier et al. (2011) suggested that aerosol layer at the tropopause of Asia could be sulfur and/or organics, considering that Asian pollutants consisted of black carbon, organic carbon, SO_2, and NO_x (Park et al., 2009; Randel et al., 2010). Weigel et al. (2011) analyzed the volatility of aerosols obtained from in situ airborne measurements and reported that about 75–90 % of the particles in the tropical tropopause layer were volatile, but this study did not give any detailed analyses of chemical composition of aerosols. Bourgeois et al. (2012) showed, by using the ECHAM5.5-HAM2 model, that sulfate, water, and OC contributed, respectively, 53%, 29%, and 11% to aerosol extinction in the vicinity of the

tropical tropopause layer. The ECHAM5.5-HAM2 model used by Bourgeois et al. (2012) simulated all major aerosol species in the atmosphere except for nitrate.

Few previous studies have examined nitrate aerosol in the UTLS, although nitrate is expected to be important for the following reasons. First, emissions of precursors of nitrate, such as NO_x and NH_3, are high over India, Southeast Asia, and China (Streets et al., 2003; Datta et al., 2012; Huang et al., 2012). Second, simulated nitrate concentrations are high over those regions (Liao and Seinfeld, 2005; Mu and Liao, 2014; Lou et al., 2014). Third, measured concentrations of nitrate are comparable to or larger than those of sulfate at rural and urban sites in the SASM region. Shrestha et al. (2000) carried out measurements of aerosols at Phortse, Nepal, during September 1996–November 1997, and showed that the average concentration of nitrate during the monsoon season (June-September) was 0.34 μg m^{-3}, higher than that of sulfate (0.17 μg m^{-3}). Decesari et al. (2010) reported, on the basis of measurements at the Nepal Climate Observatory-Pyramid from 2006 to 2008, that the concentrations of nitrate and sulfate were 0.37 μg m^{-3} and 0.50 μg m^{-3}, respectively, during the monsoon season. Chatterjee et al. (2010) measured aerosols at a high altitude station in northeastern Himalayas during January-December 2005. They found that the average concentrations of fine-mode nitrate and sulfate were 3.31±2.25 μg m^{-3} and 3.80±2.9 μg m^{-3}, respectively. At Lahore, an urban site in Pakistan, the observed daytime nitrate concentration of 21.8 μg m^{-3} was also higher than sulfate concentration of 12.6 μg m^{-3} (Lodhi et al., 2009), as the observations were averaged over November 2005 to March 2006. Fourth, the low temperatures in the UTLS would favor

nitrate formation (Seinfeld and Pandis, 2006). Therefore, it is of interest to take nitrate aerosol into consideration when we examine aerosols in the UTLS.

In this work we simulate nitrate aerosol and its contribution to aerosol concentrations in the UTLS over the TP (70–105°E, 25–40°N) and the SASM region (70–105°E, 10–25°N) by using the global chemical transport model GEOS-Chem driven by the assimilated meteorological fields. These regions of interest are shown in Fig. 1. Simulated surface-layer aerosol concentrations are compared with ground-based observations, and simulated aerosols in the UTLS are evaluated by using the Stratospheric Aerosol and Gas Experiment II (SAGE II) satellite data. Section 2 is a brief description of the GEOS-Chem model and numerical experiment. Section 3 presents the simulation and evaluation of distributions and concentrations of HNO_3 and O_3 to show model's capability in simulating the NO_x-O_3-HNO_3 cycle over the studied regions. Section 4 shows simulated aerosols and Section 5 presents the simulated contribution of nitrate to aerosol concentrations in the UTLS over the TP and the SASM region. Section 6 discusses the mechanisms for high concentrations of nitrate in the UTLS. Section 7 discusses the impacts of uncertainties in surface-layer aerosol concentrations on simulated nitrate in the UTLS.

2 Model description and numerical experiment

2.1 GEOS-Chem model

We simulate gas-phase species and aerosols using the global chemical transport model GEOS-Chem (version 9-01-03, http://geos-chem.org) driven by the GEOS-5 assimilated meteorological fields from the Goddard Earth Observing System of the NASA Global Modeling and Assimilation Office. The

version of the model used here has a horizontal resolution of 2° latitude by 2.5° longitude and 47 vertical layers extending from the surface to 0.01 hPa. Over the TP and the SASM region, the model has about 34 layers in the troposphere and 12 layers in the stratosphere.

The GEOS-Chem model has a fully coupled treatment of tropospheric NO_x-CO-hydrocarbon-aerosol chemistry and aerosols including sulfate (SO_4^{2-}), nitrate (NO_3^-), ammonium (NH_4^+), organic carbon (OC), black carbon (BC) (R. J. Park et al., 2003; 2004; Pye et al., 2009), mineral dust (Fairlie et al., 2007), and sea salt (Alexander et al., 2005; Jaeglé et al., 2011). Anthropogenic aerosols are treated as bulk mass concentrations (particles of SO_4^{2-}, NO_3^-, NH_4^+, BC, and OC are not size-resolved). Sea Salt mass is simulated for two size bins (0.1–0.5 and 0.5–8 μm) and mineral dust is simulated for four size bins (0.1–1.0, 1.0–1.8, 1.8–3.0, and 3.0–6.0 μm). Both BC and OC consist of hydrophilic and hydrophobic fractions in the model. It is assumed that 80% of BC and 50% of OC emitted from all primary sources are hydrophobic (Cooke et al., 1999; Chin et al., 2002; Chung and Seinfeld, 2002), which become hydrophilic with an e-folding time of 1.2 days following Cooke et al. (1999) and Chin et al. (2002). All secondary OC is assumed to be hydrophilic. Hydrophilic fractions of both BC and OC aerosols are assumed to be fully soluble.

The gas-aerosol partitioning of nitric acid and ammonium is calculated using the ISORROPIA II thermodynamic equilibrium module (Fountoukis and Nenes, 2007). In the version of the GEOS-Chem model used in this work, ions considered in ISOROPIA II include $H^+/Na^+/NH_4^+/Cl^-/SO_4^{2-}/HSO_4^-/NO_3^-/OH^-$. The two-way coupling between aerosols and gas phase chemistry provides consistent chemical fields for aerosol simulation and aerosol mass for

heterogeneous processes and calculations of gas-phase photolysis rates. Heterogeneous reactions include hydrolysis of N_2O_5 (Evans and Jacob, 2005), irreversible absorption of NO_3 and NO_2 on wet aerosols (Jacob, 2000), and the uptake of HO_2 by aerosols (Liao and Seinfeld, 2005; Thornton et al., 2008). Aerosol species are treated as an external mixture in the calculation of aerosol optical properties.

With respect to chemistry in the stratosphere, stratospheric O_3 concentrations are calculated using the linearized parameterization scheme (McLinden et al., 2000). The monthly mean production rates and loss frequencies of other stratospheric species (including long-lived species such as CFCs and N_2O) use those from NASA Global Modeling Initiative (GMI) Combo simulations (Duncan et al., 2007; Considine et al., 2008; Murray et al., 2012).

Convective transport in GEOS-Chem mimics that in the parent GEOS general circulation model (GCM) (Hack, 1994; Zhang and McFarlane, 1995), which accounts for updraft, downdraft, and entrainment mass fluxes for deep and shallow convection (Wu et al., 2007). The aerosol wet deposition scheme in the GEOS-Chem follows that of Liu et al. (2001). For the scavenging of aerosols, SO_4^{2-}, NO_3^-, NH_4^+, and hydrophilic OC and hydrophilic BC aerosols are assumed to be fully soluble. Dry deposition follows the standard resistance-in-series model of Wesely (1989).

Global emissions of aerosols and their precursors in the GEOS-Chem follow R. J. Park et al. (2003, 2004), with anthropogenic emissions of NO_x, CO, SO_2, and non-methane volatile organic compounds (NMVOC) in Asia overwritten by David Streets' 2006 emission inventory

(http://mic.greenresource.cn/intex-b2006). Emissions of NH_3 in Asia are taken from Streets et al. (2003). Since NH_3 emissions in China showed large uncertainties in previous studies (Streets et al., 2003; Kim et al., 2006; Y. Zhang et al., 2010; Huang et al., 2011, 2012), we use the most recent estimate of NH_3 emissions in China by Huang et al. (2012), which is 9.8 Tg yr^{-1}, instead of 13.5 Tg yr^{-1} from Streets et al. (2003). Table 1 summarizes the annual emissions of NO_x, SO_2, NH_3, OC, and BC in Asia domain (60–155°E, 10–55°N).

Natural NO_x emissions from lightning are calculated using the scheme described by Sauvage et al. (2007) and Murray et al. (2012), and those from soil are simulated following Wang et al. (1998). Natural NH_3 emissions from soil, vegetation, and the oceans are taken from the Global Emissions Inventory Activity inventory (Bouwman et al., 1997). Biomass burning emissions are from the monthly Global Fire Emissions Database (GFED v3) driven by satellite observations of fire activity (van der Werf et al., 2010). Biogenic VOC (volatile organic compounds) emissions are calculated from the Model of Emissions of Gases and Aerosols from Nature (Guenther et al., 2006).

The monthly variations of emissions of SO_2 and NO_x follow Wang et al. (2013) and those of BC and OC follow Lou et al. (2014). The monthly scaling factors for NH_3 emissions follow the global inventory described in Fisher et al. (2011). Monthly variations of emissions (anthropogenic plus natural emissions) of NO_x SO_2, NH_3, OC, and BC over Asia are displayed in Fig. 2. The emissions of NH_3 are the highest in June as a result of the agriculture practice and high temperatures (Wang et al., 2013).

2.2 Numerical experiment

To examine the contribution of nitrate to aerosol concentrations in the UTLS over the TP/SASM region, we simulate aerosol concentrations by using the emissions of and meteorological fields of year 2005. Year 2005 is chosen so that we can use the observational datasets for this year from SAGE II and MLS, as described in Sects. 3 and 4. Following Rasch et al. (2008), we perform a 10-year spin-up run to generate the initial conditions (to allow the stratospheric species to reach quasi-steady state conditions). We would consider that the tropospheric simulation can be representative of year 2005 but stratosphere simulation should represent a multi-year average, because the production rates and loss frequencies in the stratosphere are the averages over years of 2004–2010 (http://wiki.seas.harvard.edu/geos-chem/index.php/ Stratospheric_ chemistry).

3 Simulated concentrations of HNO_3 and O_3 and model evaluation

Nitrate aerosol forms when nitric acid (HNO_3) reacts with alkaline gases (for example, ammonia) in the atmosphere (Seinfeld and Pandis, 2006). HNO_3, as the important precursor of nitrate, is the major oxidation product of nitrogen oxides (NO_x = NO+NO_2) (Seinfeld and Pandis, 2006). To show the model's capability in simulating the NO_x-O_3-HNO_3 cycle over the studied regions, we present and evaluate the simulated HNO_3 and O_3 in this section.

Simulated mixing ratios of HNO_3 and O_3 in the UTLS are evaluated by using datasets from the limb viewing satellite instrument of Microwave Limb Sounder (MLS, version 3.3, level 2, ftp://acdisc.gsfc.nasa.gov/data/s4pa///Aura_MLS_Level2/). The MLS datasets provide valuable information on atmospheric compositions in the UTLS

(Waters et al., 2006). For HNO_3, the MLS provides scientifically useful datasets for 215 to 1.5 hPa, with a vertical resolution of 3–4 km and a horizontal resolution of 400–500 km. Since further evaluations are needed for datasets at altitudes with pressures higher than 215 hPa (Livesey et al., 2011), we use only datasets for pressures lower than that. For O_3, the MLS provides scientifically useful datasets for 261 to 0.02 hPa, with a vertical resolution of 2.5–3 km and a horizontal resolution of 300–400 km in the UTLS (Santee et al., 2007; Livesey et al., 2011). The uncertainties of the MLS HNO_3 and O_3 datasets in the UTLS are discussed in Livesey et al. (2011).The MLS data HNO_3 product at 100 hPa represents an average of a 3–4 km layer reaching from below the tropopause layer into the lower stratosphere (Duncan et al., 2007). The data screening is conducted strictly according to the instructions of Livesey et al. (2011). For comparison with the MLS observations, the simulated HNO_3 and O_3 mixing ratios are converted to $\hat{\mathrm{x}}$, following the method of Livesey et al. (2011):

$$\hat{\mathrm{x}} = \mathrm{x_a} + \mathrm{A}\,(\mathrm{x} - \mathrm{x_a})$$

where A is the averaging kernel matrix of the MLS, x is the modeled vertical profile of HNO_3 or O_3 interpolated at the vertical grid of MLS, and $\mathrm{x_a}$ is the HNO_3 or O_3 prior profile of MLS.

3.1 HNO_3

Figure 3(a) shows the simulated global distribution of HNO_3 concentrations averaged over June-August of 2005. Concentrations of HNO_3 exceed 1 ppbv over the industrialized areas such as Europe, North America, central and eastern Asia, and over biomass burning regions in the tropics, in agreement with the distributions and magnitudes reported in Liao et al. (2003). Over South

298 Asia, simulated HNO_3 concentrations are high (0.3–1 ppbv) in the northern
299 Indian subcontinent, because the emissions of NO_x and NH_3 are high in this
300 region (Streets et al., 2003; Zhang et al., 2009; Datta et al., 2012).

301 Figures 4(a)-4(b) show the simulated HNO_3 concentrations in the UTLS
302 averaged over June-August of 2005. Since the tropopause is located at
303 70–150 hPa (12–15 km) over the TP/SASM region (Li et al., 2005; Bian et al.,
304 2011b; Fadnavis et al., 2014), we choose the vertical layers of 200 hPa and
305 100 hPa to represent the UTLS. At both 200 hPa and 100 hPa, the highest
306 HNO_3 concentrations are simulated to occur in the high latitude regions in the
307 Northern Hemisphere (NH) (Fig. 4(a) and Fig. 4(b)). Simulated HNO_3
308 concentrations at 100 hPa are low over the region of 40–100°E and 10–30°N,
309 which is part of the anticyclone region defined in Fig. 1. Figure 4(c) shows the
310 latitude-altitude cross section of simulated seasonal mean HNO_3 mixing ratios
311 averaged over 70–105°E. In boreal summer, the highest HNO_3 mixing ratios
312 are simulated to occur at 30 hPa over the Polar Regions in both hemispheres.
313 Over high latitudes, HNO_3 concentrations in the Southern Hemisphere (SH)
314 are simulated to be higher than those in the NH.

315 To evaluate the simulated HNO_3, Figures 4(d)-4(f) show HNO_3
316 concentrations in the UTLS from MLS that are averaged over June-August of
317 2005. At 200 and 100 hPa altitudes, the observed HNO_3 mixing ratios are high
318 in the high latitudes in the NH, which are captured by the GEOS-Chem model.
319 The observed HNO_3 at 100 hPa exhibits low values of less than 400 pptv over
320 30–100°E and 10–30°N in the Asian monsoon anticyclone region (Fig. 4(e)). At
321 100 hPa, the observed HNO_3 mixing ratio averaged over the TP/SASM region
322 (70–105°E, 10–40°N) is 335.4 pptv, which is lower than the simulated value of

372.6 pptv. Considering all the grid cells with MLS HNO_3 data available, the simulated seasonal mean HNO_3 concentrations show normalized mean bias (NMB) of +11.1 % at 100 hPa over the TP/SASM region in summer of year 2005. The observed pattern of the HNO_3 vertical distribution (Fig. 4(f)) is also captured by the GEOS-Chem model (Fig. 4(c)). The distributions of HNO_3 in the UTLS are associated with the Brewer-Dobson circulation proposed by Brewer (1949) and Dobson (1956), traveling upwards across the tropopause to the stratosphere at the equator and downwards to the troposphere near the Polar region.

3.2 O_3

Figure 3(b) shows the global distribution of simulated summertime surface-layer O_3 concentrations. Simulated O_3 concentrations are in a range of 40–70 ppbv over Europe, North America, China, and the biomass burning region of South Africa. Our model results agree closely with the simulated distributions and magnitudes reported in Mickley et al. (1999), Collins et al., (2000), Liao et al. (2003), Wu et al., (2008), Zeng et al. (2008), and Fadnavis et al. (2014). Fadnavis et al. (2014) also presented aircraft measurements over India in September of 2010 during the Cloud Aerosol Interaction and Precipitation Enhancement Experiment (CAIPEEX). Our simulated O_3 concentrations of 30–40 ppbv over India agree with the CAIPEEX measurements.

Figures 5(a)-5(b) show the simulated O_3 concentrations in the UTLS averaged over June-August of 2005. The distributions of O_3 concentrations in the UTLS are similar to those of HNO_3, with elevated values in the high latitudes of the NH. Relatively low O_3 mixing ratios of less than 200 ppbv are

simulated at 100 hPa over 10–30°N, 20–110°E, within the anticyclone region defined in Fig. 1. Our simulated distributions and magnitudes of O_3 agree with those reported in Bian et al. (2011b), which examined the summertime distributions of O_3 in the UTLS during 2005–2009 by using the MLS version 2.2 level 2 products (Livesey et al., 2008). Because the background O_3 concentrations are generally high in the UTLS and the stratosphere, the low O_3 concentrations in the UTLS over the TP/SASM region are caused by the deep convection that transports O_3-poor air upward (Fu et al., 2006; Randel and Park, 2006; Park et al., 2007; Bian et al., 2011b). Figure 5(c) displays the latitude-altitude cross section of seasonal mean O_3 mixing ratios averaged over 70–105°E. As a result of the Brewer-Dobson circulation, O_3 concentrations in the UTLS are lower over the tropics than in the Polar Regions, even though the maximum O_3 concentrations are located around 10 hPa over the tropics (Brewer, 1949). Our simulated O_3 concentrations in the UTLS agree well with the measurements from MLS (Fig. 5(d)-5(f)). At 100 hPa, simulated and MLS observed O_3 mixing ratios averaged over the TP/SASM region (70–105°E, 10–40°N) are 151.7 and 146.6 ppbv, respectively. Compared to MLS observations, simulated O_3 concentrations at 100 hPa have a NMB of +3.5 % over the TP/SASM region in summer of 2005. Our simulated global STE of O_3 is 420 Tg yr^{-1}, which is within the range reported in previous studies (475±120 Tg yr^{-1} in McLinden et al. (2000), 420 Tg yr^{-1} in Škerlak et al. (2014), and 556±154 Tg yr^{-1} in Stevenson et al. (2006)).

In addition to the comparisons against MLS products, the simulated O_3 profiles are compared with balloon-borne sonde measurements in Fig. 6. The measurements were carried out at Kunming (KM, 102.7°E, 25.0°N) in August

of 2009 and 2012, and at Lhasa (LH, 91.1°E, 29.7°N) in August of 2010 and 2013. The uncertainties of the observed O_3 mixing ratios were estimated to be within 5–10% (Bian et al. 2012). The comparisons with multi-year observations show that the model can reproduce the vertical distributions of O_3 above 12 km in Kunming and Lhasa. At 100 hPa, the simulated monthly mean O_3 mixing ratio in KM is 112.6 ppbv, and the observed value is 124.2 ppbv in 2009 and 113.5 ppbv in 2012. In LH, the simulated monthly O_3 mixing ratio at 100 hPa is 152.6 ppbv, and the observed O_3 mixing ratio at that altitude is 142.4 ppbv in 2010 and 167.9 ppbv in 2013. The magnitudes of O_3 mixing ratios from these balloon-borne sonde measurements support those from MLS; O_3 mixing ratios in the UTLS are less than 200 ppbv over the TP/SASM region.

4 Simulated aerosols and model evaluation

4.1 Simulated aerosols

Figure 7 (a) shows the simulated surface-layer concentrations of SO_4^{2-}, NO_3^-, NH_4^+, OC, BC, and $PM_{2.5}$ (the sum of the mass of SO_4^{2-}, NO_3^-, NH_4^+, BC, and OC aerosols) averaged over June-August of year 2005. As expected, simulated aerosol concentrations are high over polluted regions such as India and eastern China as a result of the high anthropogenic emissions of aerosol precursors and aerosols (Streets et al., 2003; Huang et al., 2012). Over the TP/SASM region (70–105°E, 10–40°N), the average concentrations of SO_4^{2-}, NO_3^-, NH_4^+, BC, and OC are 1.70, 0.94, 0.85, 0.30, and 0.94 μg m^{-3}, respectively. NO_3^- is simulated to be of secondary importance at the surface over the region of our interest. The simulated distributions and magnitudes of these aerosol species are similar to those reported in Wang et al. (2013) and

Mu and Liao (2014).

Figures 7(b) and 7(c) also show the simulated concentrations of SO_4^{2-}, NO_3^-, NH_4^+, OC, BC, and $PM_{2.5}$ in the UTLS. Elevated concentrations of SO_4^{2-}, NO_3^-, NH_4^+, OC, BC and $PM_{2.5}$ are simulated over the TP and Plateau south slope at 200 hPa altitude, and extend from eastern Mediterranean to western China at 100 hPa. The simulated enhanced concentrations of SO_4^{2-}, OC, and BC at 100 hPa over the anticyclone region (20–120°E, 10–40°N) agree with previous observational and modeling studies (Lelieveld et al., 2001; Li et al., 2005; Fadnavis et al., 2013). Li et al. (2005) reported elevated CO concentrations in the upper troposphere over the TP, on the basis of both MLS measurements and the GEOS-Chem simulation for September 2004. Fadnavis et al. (2013) also simulated maximum concentrations of SO_4^{2-}, OC, BC, and mineral dust aerosols in the UTLS during the Asian summer monsoon season owing to convective uplifting of the boundary layer pollutants. With NO_3^- aerosol accounted for in our simulation, NO_3^- is simulated to be the most dominant aerosol species in the UTLS over the TP/SASM region, followed by SO_4^{2-}, NH_4^+, OC, and BC. At 100 hPa, the averaged concentrations of SO_4^{2-}, NO_3^-, NH_4^+, OC, and BC over the TP/SASM region (70–105°E, 10–40°N) region are 0.026, 0.069, 0.014, 0.011, and 0.002 μg m^{-3}, respectively.

4.2 Comparisons of simulated aerosol concentrations with in-situ observations

The simulated aerosol concentrations in East Asia in the GEOS-Chem model have been evaluated in previous studies (L. Zhang et al., 2010; Fu et al., 2012; Jeong and Park, 2013; Jiang et al., 2013; Wang et al., 2013; Lou et al., 2014). Here we are focused on the evaluation of aerosols in the South Asian

monsoon region. For lack of publicly accessible in situ measurements of summertime aerosols in South Asia monsoon area, we compiled monthly or seasonal mean measured concentrations of each aerosol species based on measurements reported in the literature (see Table S1 in the Supplementary Material). These measurements were carried out over years of 1992–2010. The locations of sites with measurements available are shown in Fig. 8(a). Most sites are located in the upwind directions of the TP, with pollutants that can be transported to the UTLS during the South Asian summer monsoon season. The observed PM_{10} concentrations listed in Table S1 are multiplied by 0.6 to convert to $PM_{2.5}$ for model evaluation, following the suggestions in Zhang et al. (2002) and Chatterjee et al. (2010).

Figures 8(b)–8(f) show the scatterplots of simulated versus observed seasonal mean aerosol concentrations. Compared with measurements, simulated SO_4^{2-}, NO_3^-, NH_4^+, OC and BC have NMBs of –17.0%, +38.8%, +42.0%, –69.7% and –41.0%, respectively, as the concentrations of all seasons are considered. The correlations between model results and observations have *R* values of 0.49–0.85 for all aerosol species, indicating that the model is capable of capturing the spatial distributions and seasonal variations of each aerosol species in the South Asian monsoon region despite the biases in concentrations. If we consider simulated and measured concentrations for JJA alone, the simulated concentrations of SO_4^{2-}, NO_3^-, NH_4^+, OC and BC exhibit seasonal NMBs of –14.7%, +51.5%, +74.9%, –57.2% and –32.2%, respectively, and the values of *R* are in the range of 0.24–0.85. Note that the measurements of NO_3^- and NH_4^+ are quite limited in terms of the number of samples, and the discrepancies between model results and

448 measurements may also arise from the mismatch of the model year 2005 with
449 the years of 1992–2010 with observations available.

450 **4.3 Comparisons of simulated aerosol extinction coefficients with SAGE**
451 **II datasets**

452 Satellite datasets from the Stratospheric Aerosol and Gas Experiment II
453 (SAGE II, https://eosweb.larc.nasa.gov/project/sage2/sage2_v620_table) are
454 used to evaluate the simulated aerosol extinction in the UTLS. The SAGE II
455 instrument was launched in October 1984 aboard the Earth Radiation Budget
456 Satellite (ERBS) and terminated on 8 September 2005 (McCormick et al. 1987;
457 Chu et al. 1989). The datasets used here are aerosol extinction coefficients at
458 525 nm from the version 6.20 SAGE retrievals, covering from 0.5 to 40 km with
459 a vertical resolution of 0.5 km. Many validation studies have been conducted
460 on the SAGE II aerosol data (Russell and McCormick, 1989; Oberbeck et al.,
461 1989; Wang et al., 1989), which indicated that extinction coefficients have
462 uncertainties of 20–30%. The extinction coefficients of aerosols in the
463 GEOS-Chem model are calculated using aerosol mass concentration,
464 extinction efficiency, effective radius, particle mass density, and the assumed
465 aerosol size distribution (Drury et al., 2010). The hygroscopic growth of each
466 aerosol species with relative humidity is accounted for, using the hygroscopic
467 growth factors listed in Martin et al. (2003).

468 Figure 9(a) presents the simulated monthly mean distribution of aerosol
469 extinction coefficients at 100 hPa for July of 2005. At 100 hPa, the simulated
470 aerosol extinction coefficients are relatively high over the anticyclone region,
471 where anthropogenic aerosol species (Fig. 7) and natural aerosols such as
472 mineral dust and sea salt contribute to aerosol extinction coefficients in

summer. Note that the contributions of sulfate, nitrate, ammonium, OC, sea salt, and mineral dust are all considered when we calculate aerosol extinction coefficients. Aerosol extinction coefficients are simulated to be 1.2–2×10^{-3} km^{-1} at 100 hPa over the Asian continent and Indian Ocean (20°S–30°N, 30°–105°E). These values agree closely with aerosol extinction coefficients measured at Naqu during August of 2011 for the same altitude, the maximum of which was 2.4×10^{-3} km^{-1} (He et al., 2014). Vernier et al. (2011) also identified this Asian aerosol layer with high SR at 100 hPa by observations of CALIPSO for JJA of 2006–2008.

Figure 9(b) displays the monthly mean vertical profiles of aerosol extinction coefficients averaged over the Asian monsoon anticyclone region (20–120°E 10–40°N) (Fig. 1) for July of 2005. The SAGE II datasets are available for July only in 2005. The profiles from SAGE II and the GEOS-Chem simulation are all shown. The vertical distributions of aerosol extinction coefficients “with nitrate” and “without nitrate” are both from the baseline run with full chemistry. The vertical distribution of aerosol extinction coefficient “with nitrate” (or “without nitrate”) indicates that the contribution of nitrate aerosol to aerosol extinction is (or is not) accounted for. Accounting for all aerosol species, the GEOS-Chem model reproduces well the aerosol extinction coefficients above 10 km, but the discrepancies are rather large in altitudes less than 10 km. Note that the uncertainties in satellite datasets increase as the altitude decreases (Vanhellemont et al., 2008；Kulkarni and Ramachandran, 2015), and the missing data in the lower troposphere along the satellite trajectories over the region of our interest also contribute to the discrepancies

Comparisons of profiles of aerosol extinction coefficients with and without

498 nitrate aerosol indicate that the profiles show small differences in altitudes less
499 than 6 km but large discrepancies from 6 km to the tropopause. With nitrate
500 aerosol accounted for, the simulated aerosol extinction coefficients agree
501 closely with SAGE II datasets in the UTLS (averaged over 14–16 km, the
502 simulated value is 8.6×10^{-4} km^{-1} while the observed value is 8.0×10^{-4} km^{-1}).
503 Without nitrate aerosol, the simulated aerosol extinction coefficient at 14–16
504 km altitude is 1.5×10^{-4} km^{-1}, which underestimates the aerosol extinction
505 coefficient by 82.6% compared to that calculated with all the aerosol species.
506 These comparisons of extinction coefficients with and without nitrate aerosol
507 suggest that nitrate aerosol plays an important role in aerosol extinction in the
508 UTLS over the region of our interest.
509
510 **5 Contribution of nitrate to aerosol concentrations in the UTLS**
511 Since nitrate aerosol is simulated to be the most abundant aerosol species in
512 the UTLS over the TP/SASM region, we analyze the contribution of nitrate to
513 $PM_{2.5}$ concentration (C_{NIT}=nitrate concentration/$PM_{2.5}$ concentration) in this
514 section. Figure 10 shows the simulated seasonal mean distributions of C_{NIT} for
515 June-August of year 2005. At the surface layer (Fig. 10(a)), simulated high C_{NIT}
516 values are located over the areas with high nitrate concentrations (India and
517 eastern China) as well as the oceans where NO_3^- also forms on sea salt and
518 mineral dust particles (Arimoto et al., 1996; Nakamura et al., 2005; George and
519 Nair, 2008). Over the TP/SASM region, the C_{NIT} values in JJA are 5–35% at the
520 surface, 25–50% at 200 hPa (Fig. 10(b)), and could exceed 60% at 100 hPa
521 (Fig. 10(c)). The latitude-altitude cross section of C_{NIT} (Fig. 10(d)) shows that
522 C_{NIT} over 20–40°N increases with altitude and reaches maximum values

around the extratropical tropopause.

Table 2 lists the mean concentrations of SO_4^{2-}, NO_3^-, NH_4^+, BC and OC, and their contributions to $PM_{2.5}$ during summertime of 2005 over the TP/SASM, TP, and SASM regions. Over the TP/SASM region, SO_4^{2-}, NO_3^-, NH_4^+, BC and OC are simulated to contribute 35.9%, 19.8%, 18.1%, 6.4%, and 19.8%, respectively, to $PM_{2.5}$ mass concentration at the surface layer. The contributions increase significantly in the UTLS. The largest C_{NIT} is simulated in the SASM region at 100 hPa, where NO_3^- accounts for 60.5% of $PM_{2.5}$ mass concentration. The high C_{NIT} values indicate that NO_3^- plays an important role in the aerosol layer in the UTLS over the TP/SASM region.

Considering the large uncertainties in simulated sea salt (Jaeglé et al., 2011) and mineral dust (Fairlie et al., 2007) aerosols, we tend to be focused on anthropogenic aerosol species (SO_4^{2-}, NO_3^-, NH_4^+, BC, and OC) in this work. In our model, concentrations of sea salt (or mineral dust) are simulated to be 1.0–1.7 ng m^{-3} (or 5.0–7.0 ng m^{-3}) over the studied region in the summer of 2005, which contribute less than 1.2% (or 5.0%) to total aerosol mass at 100 hPa. Therefore the consideration of sea salt and mineral dust can slightly reduce C_{NIT} values, but C_{NIT} values at 100 hPa are still as high as 45-65% over the TP/SASM region in summer.

6 Mechanisms for high nitrate concentrations in the UTLS

6.1 Upward transport of nitrate from the lower troposphere

The intense convective transport of chemical species into the UTLS over the TP/SASM region during summertime has been widely discussed in previous studies (Randel et al., 2010; Bian et al., 2011a; Fadnavis et al., 2013, 2014;

548 Qie et al., 2014; He et al., 2014), evidenced by both the satellite observations
549 (Fu et al., 2006; Luo et al., 2011) and the calculation of the outgoing long-wave
550 radiation which is a convective proxy over the region (Randel and Park, 2006;
551 Park, et al., 2007; Fadnavis et al., 2013). Since nitrate aerosol is simulated to
552 be of secondary abundant aerosol species in the surface layer over the
553 TP/SASM region (Fig. 7), the vertical mass transport through the deep
554 convection in this region contributes to the accumulation of NO_3^- in the UTLS.
555 Figure 11 shows the latitude-altitude cross sections of simulated
556 concentrations of SO_4^{2-} and NO_3^- averaged over 70–105°E in June-August of
557 2005, together with the wind vectors obtained from the European Centre for
558 Medium-Range Weather Forecasts (ECMWF) ERA-Interim Reanalysis data.
559 Note that the assimilated GEOS-5 meteorological fields do not have vertical
560 winds
561 (http://wiki.seas.harvard.edu/geos-chem/index.php/List_of_GEOS-5_met_field
562 s), so we use the ECMWF reanalysis wind fields to do the analysis here. High
563 values of aerosol concentrations are found on the south slope of the
564 Himalayas, where the deep convection exists. Although both SO_4^{2-} and NO_3^-
565 are transported upward to the extratropical tropopause, the details of the
566 vertical distributions are different. At altitudes higher than 8 km, the
567 concentrations of NO_3^- do not decrease with altitude as quickly as those of
568 SO_4^{2-}, and the concentrations of NO_3^- over 10–40°N are higher than those of
569 SO_4^{2-}.

570 The chemical mechanisms for the formation of SO_4^{2-}, NO_3^-, and NH_4^+
571 aerosols in the GEOS-Chem model were described in R. J. Park et al. (2004),
572 which are comprehensive and have been used extensively in previous studies

to simulate these three aerosol species (R. J. Park et al., 2004; Pye et al., 2009; L. Zhang et al., 2010; Zhu et al., 2012; Jiang et al., 2013; Lou et al., 2014). Sulfate aerosol forms from gas-phase oxidation of SO_2 by OH and from in-cloud oxidation of SO_2 by O_3 and H_2O_2. Nitrate forms from the partitioning of HNO_3 between gas and aerosol phases, which is calculated by the ISORROPIA II thermodynamic equilibrium module (Fountoukis and Nenes, 2007) in the GEOS-Chem model. HNO_3 is produced by the reaction of NO_2 with OH during daytime and by hydrolysis of N_2O_5 on aerosol surfaces at night (Table 3). The chemical mechanisms for SO_4^{2-} and NO_3^- have different sensitivity to meteorological conditions. During the vertical transport, temperature decreases, which reduces the gas-phase oxidation of SO_2 (Yao et al., 2002; Seinfeld and Pandis 2006) but promotes the formation of NO_3^- by shifting gas-particle equilibria (Dawson et al., 2007; Liao et al., 2009). Dawson et al. (2007) examined the sensitivities of sulfate and nitrate concentrations to temperature by using the Particulate Matter Comprehensive Air Quality Model with extensions (PMCAMx). The sensitivity test was performed by fixing all meteorological parameters but perturbing temperature. Their sensitivity simulations showed that the increases in temperature led to increases in sulfate concentrations and decreases in nitrate concentrations. Compared to nitrate, sulfate concentrations showed smaller sensitivity to temperature changes (Dawson et al., 2007); as temperature increased, nitrate concentrations decreased by 19% K^{-1} and 17% K^{-1} in January and July respectively, while sulfate concentration increased by 0.12% K^{-1} and 1.3% K^{-1} in January and July, respectively. Therefore the different chemical mechanisms for SO_4^{2-} and NO_3^- formation contribute to the differences in their vertical

598 distributions.

599 **6.2 Net chemical production of HNO_3 during the vertical transport**

600 As mentioned above, the formation of gas-phase HNO_3 and the
601 partitioning of HNO_3 between gas and aerosol phases are the two major
602 chemical processes that influence NO_3^- concentrations. The ability of the
603 GEOS-Chem model to simulate gas-phase HNO_3 has been evaluated in
604 Section 3.1 (by comparisons of our model results with MLS observations and
605 concentrations from previous modeling studies). Major reactions for the
606 production and loss of HNO_3 are listed in Table 3. Figure 12 shows the net
607 chemical production of HNO_3 by gas-phase reactions and heterogeneous
608 reactions (chemical production by reactions R1-R23 minus chemical loss by
609 reactions R24-R25 in Table 3) summed over the TP/SASM region. The net
610 chemical production has an overall trend of decreasing with altitude. Since
611 NO_x emissions from aircraft and lightning are located between 200–300 hPa
612 over the TP/SASM region during summer (Martin et al., 2007; Murray et al.,
613 2012; Pitari et al., 2015), net chemical production of HNO_3 shows a small peak
614 at those altitudes. The mixing ratio of HNO_3 decreases with altitude between
615 500 and 200 hPa and increases with altitude above 200 hPa. At 100 hPa, the
616 average HNO_3 mixing ratio over the TP/SASM region agrees with the values of
617 300–400 pptv over the same region shown in Fig. 4.

618 Figure 12 also shows the transport of HNO_3 over the TP/SASM region,
619 defined as convergence of horizontal flux of HNO_3 (inflow minus outflow) plus
620 convergence of vertical flux of HNO_3 (inflow minus outflow) for a specific
621 vertical model layer. At altitudes below 200 hPa, concentrations of HNO_3 over
622 the TP/SASM region are dependent on the net chemical production by

623 gas-phase reactions and heterogeneous reactions as well as the transport of
624 HNO_3.The vertical variation of the horizontal transport (the north-south and the
625 east-west transport) follows the development of the anticyclone in the upper
626 troposphere during summertime. As the altitude increases, the westerlies
627 enhance over the TP and the easterlies develop over the SASM region (see
628 Fig. 1 for our definitions of TP and SASM regions). At latitudes between 100–
629 500 hPa, vertical transport of HNO_3 occurs over the TP due to the deep
630 convection activities over the region which can arrive at 100–200 hPa (Fig. 11;
631 Fadnavis et al., 2013; Qie et al., 2014).

632 **6.3 The gas-to-aerosol conversion of HNO_3 to form nitrate during the**
633 **vertical transport**

634 NO_3^- formation from gas-to-aerosol conversion of HNO_3 is calculated by using
635 the ISORROPIA II thermodynamic equilibrium module (Fountoukis and Nenes,
636 2007). As shown in Fig. 12, the nitrate formation from gas to aerosol
637 conversion of HNO_3 peaks between 100–300 hPa, indicating that the
638 gas-aerosol partitioning plays an important role in the enhancement of nitrate
639 in the UTLS.

640 The gas-to-aerosol conversion of HNO_3 to form NO_3^- is very sensitive to
641 relative humidity (RH) and temperature (Fountoukis and Nenes 2007; Dawson
642 et al., 2007). Low temperature and high RH are favorable for NO_3^- formation.
643 Figure 13 shows the seasonal mean horizontal distributions of RH and
644 temperature at 100 hPa and the latitude-altitude cross sections of these two
645 parameters averaged over 70–105°E. RH exhibits high values in the TP/SASM
646 region, which are consistent with the high H_2O mixing ratios in this area
647 reported in Gettelman et al. (2004), M. Park et al. (2004), and Fu et al. (2006).

At 100 hPa, the locations with high RH of exceeding 45% correspond well with those with high C_{NIT} values (Fig. 10(c)). The latitude-altitude cross section of RH (Fig. 13(c)) shows that RH has high values over the places with intense upward transport (Fig. 11). For temperature, as Fig. 13(b) and 13(d) show, summertime temperatures are cold (190–200 K) at 100 hPa in the TP/SASM region, consistent with the distribution and magnitude reported for August, 2011, in He et al. (2014) on the basis of the NCEP Reanalysis data. The low temperatures over the TP/SASM region are associated with the adiabatic expansion of ascending air mass of the deep convections (Yanai et al., 1992; Park et al., 2007; He et al., 2014).

Because of the favorable conditions of RH and decreasing temperature, the gas-to-aerosol conversion of HNO_3 to form nitrate can occur during the upward transport and in the UTLS. Figure 14 shows the mass budget for nitrate aerosol within the selected box of (70–105°E, 10–40°N, 8–16 km) to see the role of nitrate formation over the TP/SASM region. The horizontal mass fluxes have a net negative value of 0.10 Tg season^{-1}, reducing nitrate aerosol in the selected box. The vertical transport and the gas-to-aerosol conversion of HNO_3 increase nitrate mass in the selected box, with values of 0.09 Tg season^{-1} and 0.11 Tg season^{-1}, respectively, indicating that the gas-to-aerosol conversion plays an important role in the enhancement of nitrate in the UTLS over the TP/SASM region. Although relatively high RH exists near the tropopause of the TP/SASM region, the air near the tropopause is still dryer compared to that in the lower altitudes. Model results show that the gas-to-aerosol partition of HNO_3 decreases with altitude between 100–300 hPa, indicating that the gas to aerosol conversion contributes to nitrate

accumulation in the UTLS mainly during the process of upward transport.

Previous studies have also reported that nitric acid trihydrates (NAT, HNO_3•$(H_2O)_3$) could form in the polar and tropical stratosphere at low temperatures through two mechanisms: (1) the homogeneous nucleation out of supercooled ternary solutions, and (2) the heterogeneous formation on ice particles (Hofmann et al., 1989; Carslaw et al., 1998; Voigt et al., 2000; Popp et al., 2006; Kirner et al., 2011). A typical NAT condensation temperature is approximate 193 K (Kirner et al., 2011). As shown in Fig. 13, the temperatures around 100 hPa over the TP/SASM region are in the range of 190–200 K, which are low enough to produce some NAT particles. However, balloon-borne measurements of depolarization ratio and backscattering ratio of aerosols at Lhasa during August-October of 1999 by Kim et al. (2003) and Tobo et al. (2007) suggested that coarse and aspherical particles such as NAT are scarce in the UTLS of the TP/SASM.

7 Sensitivities of simulated nitrate in the UTLS to anthropogenic NO_x, NH_3, and SO_2 emissions in Asia

Since simulated SO_4^{2-}, NO_3^- and NH_4^+ concentrations have, respectively, NMBs of –17.0%, +38.8%, and +42.0% on an annual mean basis and of –14.7%, +51.5%, and +74.9% in summer (Section 4.2), we perform four sensitivity simulations to examine the impacts of uncertainties in surface-layer aerosol concentrations on simulated nitrate in the UTLS. In the first three cases, anthropogenic emissions of NO_x, NH_3, and SO_2 in Asia are changed by –50%, –50%, and +20%, respectively, relative to those in our standard simulation. In the last case, anthropogenic emissions of all these three species

698 are changed simultaneously, with NO_x reduced by 50%, NH_3 reduced by 50%,
699 and SO_2 increased by 20% in Asia relative to the standard case. The purpose
700 of these sensitivity studies is to reduce NMBs of simulated surface-layer
701 concentrations of SO_4^{2-}, NO_3^- and NH_4^+ and see whether NO_3^- is still the
702 most dominant aerosol species in the UTLS. Model results from these
703 sensitivity studies for summer of 2005 are presented in Table 4.

704 As anthropogenic emissions of SO_2 in Asia are increased by 20%, the
705 NMB of simulated surface-layer SO_4^{2-} concentrations is –4.4%, which is an
706 improvement compared to the NMB of –14.7% in the standard simulation.
707 However, the increases in SO_2 emissions lead to larger NMBs of surface-layer
708 NO_3^- and NH_4^+ because of the increased formation of ammonium sulfate or
709 ammonium bisulfate. The percentage contributions of SO_4^{2-} to total aerosol
710 mass in the UTLS increase slightly by 2.7% at 200 hPa and by 1.6% at 100
711 hPa, and nitrate in the UTLS also shows small sensitivity to the change in SO_2
712 emissions.

713 With anthropogenic emissions of NO_x in Asia reduced by 50%, the NMB of
714 simulated surface-layer NO_3^- concentrations changes from +51.5% in the
715 standard simulation to –11.7% in this sensitivity run. The contribution of each
716 of SO_4^{2-}, NO_3^- and NH_4^+ aerosols to total aerosol mass in the UTLS is not
717 sensitive to this reduction in NO_x emissions at the surface; the percentage
718 contribution obtained from this sensitivity run is very close to the value
719 obtained in the standard simulation (Table 4). Similarly, in the sensitivity study
720 with NH_3 emissions reduced by 50% in Asia, simulated surface-layer
721 concentrations of NO_3^- and NH_4^+ are improved in terms of the values of NMBs,
722 but the improvement in simulated aerosol concentrations at the surface-layer

723 does not influence our conclusion of high nitrate aerosol concentration in the
724 UTLS.

725 As shown in Table 4, for the surface layer, simulated nitrate concentration
726 over the TP/SASM region decreases by 46.8% (from 0.94 μg m^{-3} to 0.50 μg m^{-3})
727 with a 50% reduction in anthropogenic NO_x emissions in Asia, and it decreases
728 by 22.3% (from 0.94 μg m^{-3} to 0.73 μg m^{-3}) when anthropogenic NH_3 emissions
729 are reduced by the same percentage, indicating that surface-layer nitrate
730 aerosol is more sensitive to anthropogenic emissions of NO_x than to those of
731 NH_3. Relative to the baseline simulation, simulated nitrate concentrations at
732 200 hPa and 100 hPa decrease, respectively, by 49.0% (from 7.57×10^{-2} μg m^{-3}
733 to 3.86×10^{-2} μg m^{-3}) and 17.7% (from 6.90×10^{-2} μg m^{-3} to 5.68×10^{-2} μg m^{-3})
734 with a 50% reduction in NH_3 emissions, whereas only by 2.1% (from 7.57×10^{-2}
735 μg m^{-3} to 7.41×10^{-2} μg m^{-3}) and 1.3% (from 6.90×10^{-2} μg m^{-3} to 6.81×10^{-2} μg
736 m^{-3}) with a 50% reduction in NO_x emissions. Over the studied region, the role
737 of NH_3 in the sulfate-nitrate-ammonium aerosol system can be quantified by
738 the gas ratio of $\mathrm{GR} = \frac{\text{free ammonia}}{\text{total nitrate}} = \frac{\mathrm{TA}-2\times\mathrm{TS}}{\mathrm{TN}}$ (Ansari and Pandis, 1998), where
739 $\mathrm{TA} = \mathrm{NH_3} + \mathrm{NH_4^+}$, $\mathrm{TS} = \mathrm{SO_4^{2-}}$, and $\mathrm{TN} = \mathrm{HNO_3} + \mathrm{NO_3^-}$. Over the TP/SASM
740 region, GR is generally positive both at the surface and in the UTLS, especially
741 over 20–40°N where deep convection exits (Fig. 11), indicating that free
742 ammonia is available to react with nitrate (Seinfeld and Pandis 2006). However,
743 GR is generally less than 1.0 above 400 hPa in summer over the TP/SASM
744 region, which indicates nitrate concentrations are most sensitive to changes in
745 NH_3 and explains the small sensitivity of nitrate aerosol to NO_x emissions in
746 the UTLS.

747 In the sensitivity study with emissions of NO_x, NH_3, and SO_2 in Asia

748 changed simultaneously, simulated surface-layer concentrations of SO_4^{2-}, NO_3^-
749 and NH_4^+ have NMBs of −8.3%, −27.0% and +55.4%, respectively, which are
750 all improved compared to those in the standard simulation. Even though nitrate
751 aerosol is now underestimated at the surface, it still accounts for 53.3% of the
752 $PM_{2.5}$ concentration at 100 hPa over the TP/SASM region in summer.

753 It should be noted that the concentrations of OC and BC are also
754 underestimated, with NMBs of −57.2% and −32.2%, respectively, in summer
755 (Section 4.2). We have done a simple calculation with the concentrations of
756 OC and BC in the UTLS multiplied by 2.3 and 1.5, respectively, and nitrate is
757 still the most dominant aerosol species in summertime in the UTLS over the
758 TP/SASM region (not shown in Table 4). Therefore the uncertainties in surface
759 aerosol concentrations do not compromise the conclusion of this study.

760

761 **8 Conclusions**

762 In this work we simulate nitrate aerosol and its contribution to aerosol
763 concentrations in the UTLS over the TP/SASM region (70–105°E, 10–40°N)
764 for summertime of year 2005, using the global chemical transport model
765 GEOS-Chem driven by the assimilated meteorological fields.

766 Simulated HNO_3 and O_3 are evaluated to show the model's ability to
767 simulate the NOx-O_3-HNO_3 cycle over the studied region. In the UTLS, both
768 the horizontal and vertical distributions of simulated HNO_3 and O_3 agree well
769 with the MLS observations. At 100 hPa, simulated seasonal mean HNO_3 and
770 O_3 mixing ratios show NMBs of +11.1 % and +3.5 %, respectively, over the
771 TP/SASM region (70−105°E, 10−40°N) in summer of year 2005, and the model
772 biases lie within the confidence range of the MLS instruments. Both simulated

773 and observed O_3 concentrations show relatively low values of less than 200
774 ppbv at 100 hPa over the TP/SASM region.

775 Averaged over the TP/SASM region, the surface-layer concentrations of
776 SO_4^{2-}, NO_3^-, NH_4^+, BC, and OC are simulated to be 1.70, 0.94, 0.85, 0.30, and
777 0.94 μg m^{-3}, respectively. Nitrate aerosol is simulated to be of secondary
778 importance near the surface over the region of our interest. Comparisons of
779 simulated aerosol concentrations with ground-based observations show that
780 simulated summertime concentrations of SO_4^{2-}, NO_3^-, NH_4^+, OC and BC have
781 NMB of –14.7%, +51.5%, +74.9%, –57.2% and –32.2%, respectively. Note that
782 the measurements of NO_3^- and NH_4^+ are quite limited in terms of the number
783 of samples.

784 Model results show elevated concentrations of SO_4^{2-}, NO_3^-, NH_4^+, OC, BC
785 and $PM_{2.5}$ in the UTLS over the TP/SASM region throughout the summer. NO_3^-
786 is simulated to be the most dominant aerosol species in the UTLS of the
787 TP/SASM region. Accounting for NO_3^- aerosol, the GEOS-Chem model
788 reproduces well the magnitude of aerosol extinctions above 10 km, as model
789 results are compared with the SAGE II measurements. The discrepancies
790 between the simulated and observed aerosol extinction coefficient are within 8%
791 in the UTLS (averaged over 14–16 km). Simulated vertical profiles of aerosol
792 extinction coefficients with and without nitrate aerosol show large
793 discrepancies from 6 km to tropopause, indicating the important role of nitrate
794 in aerosol layer in the UTLS over the TP/SASM region.

795 The contribution of NO_3^- to aerosols in the TP/SASM region is quantified
796 by C_{NIT} (the ratio of nitrate concentration to $PM_{2.5}$ concentration). Over the
797 TP/SASM region, the C_{NIT} values in summer are 5–35% at the surface, 25–

50% at 200 hPa, and could exceed 60% at 100 hPa. The mechanisms for the accumulation of nitrate in the UTLS over the TP/SASM region include vertical transport and the gas-to-aerosol conversion of HNO_3 to form nitrate. Such gas-to-aerosol conversion occurs during the upward transport and in the UTLS. The high relative humidity and low temperature associated with the deep convection over the TP/SASM region are favorable for nitrate formation.

Results from the present study indicate that nitrate is an important aerosol species in the UTLS over the TP/SASM region. Considering the scarce measurements of nitrate in the UTLS and the model uncertainties, more observational and modeling studies are needed to further explore the aerosol composition in the Asian tropopause aerosol layer. Further simulations of nitrate aerosol in the UTLS also need to account for NAT formation at low temperatures (Kirner et al., 2011) and the roles of natural aerosols, including the transport of mineral dust and sea salt to the UTLS as well as nitrate formation on these natural particles (Ma et al., 2003).

Acknowledgments. This work was supported by the National Basic Research Program of China (973 program, Grant No. 2014CB441202), the Strategic Priority Research Program of the Chinese Academy of Sciences (Grant No. XDA05100503), and the National Natural Science Foundation of China under grants 41021004, 41475137, and 91544219. We gratefully acknowledge NASA, USA, for providing the MLS and SAGE II data on their website.

References

Ansari, A. S., and Pandis, S. N.: Response of Inorganic PM to Precursor Concentrations, Environ. Sci. Technol., 32(18), 2706–2714, 1998.

Adhikary, B., Carmichael, G. R., Tang, Y., Leung, L. R., Qian, Y., Schauer, J. J., Stone, E. A., Ramanathan, V., and Ramana, M. V.: Characterization of the seasonal cycle of south Asian aerosols: A regional-scale modeling analysis, J. Geophys. Res., 112, D22S22, doi:10.1029/2006JD008143, 2007.

Alexander, B., Park, R. J., Jacob, D. J., Li, Q., Yantosca, R. M., Savarino, J., Lee, C., and Thiemens, M.: Sulfate formation in sea-salt aerosols: Constraints from oxygen isotopes, J. Geophys. Res., 110, D10307, doi:10.1029/2004JD005659, 2005.

Arimoto, R., Duce, R., Savoie, D., Prospero, J., Talbot, R., Cullen, J., Tomza, U., Lewis, N., and Ray, B.: Relationships among aerosol constituents from Asia and the North Pacific during PEM–West A, J. Geophys. Res., 101, 2011–2023, 1996.

Babu, S. S. and Moorthy, K. K.: Aerosol black carbon over a tropical coastal station in India, Geophys. Res. Lett., 29, 2098, doi:10.1029/2002GL015662, 2002.

Bano, T., Singh, S., Gupta, N., Soni, K., Tanwar, R., Nath, S., Arya, B., and Gera, B.: Variation in aerosol black carbon concentration and its emission estimates at the mega-city Delhi, Int. J. Remote Sens., 32, 6749–6764, 2011.

Bian, J., Yan, R., and Chen, H.: Tropospheric Pollutant Transport to the Stratosphere by Asian Summer Monsoon, Chinese Journal of Atmospheric Sciences, 35, 897–902, 2011a.

Bian, J., Yan, R., Chen, H., Lü, D., and MASSIE, S. T.: Formation of the Summertime Ozone Valley over the Tibetan Plateau: The Asian Summer Monsoon and Air Column Variations, Adv. Atmos. Sci., 28, 1318–1325, 2011b.

Bian, J., Pan, L. L., Paulik, L., Vömel, H., Chen, H., and Lü, D.: In situ water vapor and ozone measurements in Lhasa and Kunming during the Asian summer monsoon, Geophys. Res. Lett., 39, L19808, doi:10.1029/2012GL052996, 2012.

Bourgeois, Q., Bey, I., and Stier, P.: A permanent aerosol layer at the tropical tropopause layer driven by the intertropical convergence zone, Atmos. Chem. Phys. Discuss., 12, 2863–2889, 2012.

Bouwman, A., Lee, D., Asman, W., Dentener, F., Van Der Hoek, K., and Olivier, J.: A global high-resolution emission inventory for ammonia, Global Biogeochem. Cy., 11, 561-587, 1997.

Brewer, A. W.: Evidence for a world circulation provided by the measurements of helium and water vapour distribution in the stratosphere, Q. J. Roy. Meteor. Soc., 75, 351-363, 1949.

Carrico, C. M., Bergin, M. H., Shrestha, A. B., Dibb, J. E., Gomes, L., and Harris, J. M.: The importance of carbon and mineral dust to seasonal aerosol properties in the Nepal Himalaya, Atmos. Environ., 37, 2811–2824, 2003.

Carslaw, K., Wirth, M., Tsias, A., Luo, B., Dörnbrack, A., Leutbecher, M., Volkert, H., Renger, W., Bacmeister, J., and Peter, T.: Particle microphysics and chemistry in remotely observed mountain polar stratospheric clouds, J. Geophys. Res., 103, 5785–5796, 1998.

873 Chatterjee, A., Adak, A., Singh, A. K., Srivastava, M. K., Ghosh, S. K., Tiwari,
874 S., Devara, P. C., and Raha, S.: Aerosol chemistry over a high altitude
875 station at northeastern Himalayas, India, PloS one, 5, e11122,
876 doi:10.1371/journal.pone.0011122, 2010.
877 Chatterjee, A., Ghosh, S. K., Adak, A., Singh, A. K., Devara, P. C., and Raha,
878 S.: Effect of Dust and Anthropogenic Aerosols on Columnar Aerosol
879 Optical Properties over Darjeeling (2200 m asl), Eastern Himalayas, India,
880 PloS one, 7, e40286, doi:10.1371/journal.pone.0040286, 2012.
881 Chen, H., Bian, J., and Lü, D.: Advances and prospects in the study of
882 stratosphere-troposphere exchange, Chinese J. Atmos. Sci., 30, 813–820,
883 doi:1006-9895(2006)30:5<813:SDLCXP>2.0.TX;2-A, 2006.
884 Chin, M., Ginoux, P., Kinne, S., Torres, O., Holben, B., Duncan, B. N., Martin,
885 R. V., Logan, J. A., Higurashi, A., and Nakajima, T.:Tropospheric aerosol
886 optical thickness from the GOCART model and comparisons with satellite
887 and sunphotometer measurements, J. Atmos. Sci., 59, 461–483, 2002.
888 Chowdhury, Z., Zheng, M., Schauer, J. J., Sheesley, R. J., Salmon, L. G., Cass,
889 G. R., and Russell, A. G.: Speciation of ambient fine organic carbon
890 particles and source apportionment of $PM_{2.5}$ in Indian cities, J. Geophys.
891 Res., 112, D15303, doi:10.1029/2007JD008386, 2007.
892 Chu, W., McCormick, M., Lenoble, J., Brogniez, C., and Pruvost, P.: SAGE II
893 inversion algorithm, J. Geophys. Res., 94, 8339–8351, 1989.
894 Chung, S. H., and Seinfeld, J. H.: Global distribution and climate forcing of
895 carbonaceous aerosols, J. Geophys. Res., 107(D19), 4407,
896 doi:10.1029/2001JD001397, 2002.
897 Collins, W. J., Stevenson, D. S., Johnson, C. E., and Derwent, R. G.: The
898 European regional ozone distribution and its links with the global scale for
899 the years 1992 and 2015, Atmos. Environ., 34, 255–267, 2000.
900 Considine, D. B., Rosenfield, J. E., and Fleming, E. L.: An interactive model
901 study of the influence of the Mount Pinatubo aerosol on stratospheric
902 methane and water trends, J. Geophys. Res., 106, 27711-27727,
903 doi:10.1029/2001jd000331, 2001.
904 Considine, D. B., Logan, J. A., and Olsen, M. A.: Evaluation of
905 near-tropopause ozone distributions in the Global Modeling Initiative
906 combined stratosphere/troposphere model with ozonesonde data, Atmos.
907 Chem. Phys., 8, 2365–2385, 2008.
908 Cooke, W. F., Liousse, C., Cachier, H., and Feichter, J.: Construction of a 1°x1°
909 fossil fuel emission data set for carbonaceous aerosol and implementation
910 and radiative impact in the ECHAM-4 model, J. Geophys. Res., 104,
911 22,137–22,162, 1999.
912 Datta, A., Sharma, S., Harit, R., Kumar, V., Mandal, T., and Pathak, H.:
913 Ammonia emission from subtropical crop land area in India, Asia-Pac. J.
914 Atmos. Sci., 48, 275–281, 2012.
915 Dawson, J., Adams, P., and Pandis, S.: Sensitivity of $PM_{2.5}$ to climate in the
916 Eastern US: a modeling case study, Atmos. Chem. and phys., 7, 4295–
917 4309, 2007.
918 Decesari, S., Facchini, M., Carbone, C., Giulianelli, L., Rinaldi, M., Finessi, E.,
919 Fuzzi, S., Marinoni, A., Cristofanelli, P., and Duchi, R.: Chemical
920 composition of PM_{10} and PM_1 at the highaltitude Himalayan station Nepal
921 Climate Observatory-Pyramid (NCO-P)(5079 m asl), Atmos. Chem. Phys,
922 10, 4583–4596, 2010.

Dobson, G. M. B.: Origin and distribution of the polyatomic molecules in the atmosphere, Proceedings of the Royal Society of London. Series A, Mathematical and Physical Sciences, 187–193, 1956.

Drury, E., Jacob, D. J., Spurr, R. J., Wang, J., Shinozuka, Y., Anderson, B. E., Clarke, A. D., Dibb, J., McNaughton, C., and Weber, R.: Synthesis of satellite (MODIS), aircraft (ICARTT), and surface (IMPROVE, EPA–AQS, AERONET) aerosol observations over eastern North America to improve MODIS aerosol retrievals and constrain surface aerosol concentrations and sources, J. Geophys. Res., 115, D14204, doi:10.1029/2009JD012629, 2010.

Duncan, B., Strahan, S., Yoshida, Y., Steenrod, S., and Livesey, N.: Model study of the cross-tropopause transport of biomass burning pollution, Atmos. Chem. Phys., 7, 3713–3736, 2007.

Dutkiewicz, V. A., Alvi, S., Ghauri, B. M., Choudhary, M. I., and Husain, L.: Black carbon aerosols in urban air in South Asia, Atmos. Environ., 43, 1737–1744, 2009.

Evans, M., and Jacob, D. J.: Impact of new laboratory studies of N_2O_5 hydrolysis on global model budgets of tropospheric nitrogen oxides, ozone, and OH, Geophys. Res. Lett., 32, 10 L09813, doi:10.1029/2005GL022469, 2005.

Fadnavis, S., Semeniuk, K., Pozzoli, L., Schultz, M., Ghude, S., Das, S., and Kakatkar, R.: Transport of aerosols into the UTLS and their impact on the Asian monsoon region as seen in a global model simulation, Atmos. Chem. Phys., 13, 8771–8786, 2013.

Fadnavis, S., Semeniuk, K., Schultz, M., Mahajan, A., Pozzoli, L., Sonbawane, S., and Kiefer, M.: Transport pathways of peroxyacetyl nitrate in the upper troposphere and lower stratosphere from different monsoon systems during the summer monsoon season, Atmos. Chem. Phys. Discuss., 14, 20159–20195, 2014.

Fairlie, T. D., Jacob, D. J., and Park, R. J.: The impact of transpacific transport of mineral dust in the United States, Atmos. Environ., 41, 1251–1266, 2007.

Fisher, J. A., Jacob, D. J., Wang, Q., Bahreini, R., Carouge, C. C., Cubison, M. J., Dibb, J. E., Diehl, T., Jimenez, J. L., and Leibensperger, E. M.: Sources, distribution, and acidity of sulfate–ammonium aerosol in the Arctic in winter–spring, Atmos. Environ., 45, 7301–7318, 2011.

Fountoukis, C., and Nenes, A.: ISORROPIA II: a computationally efficient thermodynamic equilibrium model for K^+–Ca^{2+}–Mg^{2+}–NH_4^+–Na^+–SO_4^{2-}–NO_3^-–Cl^-–H_2O aerosols, Atmos. Chem. Phys., 7, 4639–4659, 2007.

Froyd, K., Murphy, D., Sanford, T., Thomson, D., Wilson, J., Pfister, L., and Lait, L.: Aerosol composition of the tropical upper troposphere, Atmos. Chem. Phys., 9, 4363–4385, 2009.

Fu, R., Hu, Y., Wright, J. S., Jiang, J. H., Dickinson, R. E., Chen, M., Filipiak, M., Read, W. G., Waters, J. W., and Wu, D. L.: Short circuit of water vapor and polluted air to the global stratosphere by convective transport over the Tibetan Plateau, P. Natl. A. Sci., 103, 5664–5669, 2006.

Fu, T. -M., Cao, J., Zhang, X., Lee, S., Zhang, Q., Han, Y., Qu, W., Han, Z., Zhang, R., and Wang, Y.: Carbonaceous aerosols in China: top–down constraints on primary sources and estimation of secondary contribution, Atmos. Chem. Phys., 12, 2725–2746, 2012.

973 Ganguly, D., Jayaraman, A., and Gadhavi, H.: Physical and optical properties
974 of aerosols over an urban location in western India: Seasonal variabilities,
975 J. Geophys. Res., 111, D24206, doi:10.1029/2006JD007392, 2006.
976 George, S. K., and Nair, P. R.: Aerosol mass loading over the marine
977 environment of Arabian Sea during ICARB: Sea-salt and non-sea-salt
978 components, J. Earth Syst. Sci., 117, 333–344, 2008.
979 George, S. K., Nair, P. R., Parameswaran, K., Jacob, S., and Abraham, A.:
980 Seasonal trends in chemical composition of aerosols at a tropical coastal
981 site of India, J. Geophys. Res., 113, D16209, doi:10.1029/2007JD009507,
982 2008.
983 Gettelman, A., Kinnison, D. E., Dunkerton, T. J., and Brasseur, G. P.: Impact of
984 monsoon circulations on the upper troposphere and lower stratosphere, J.
985 Geophys. Res., 109, D22101, doi:10.1029/2004JD004878, 2004.
986 Guenther, A., Karl, T., Harley, P., Wiedinmyer, C., Palmer, P., and Geron, C.:
987 Estimates of global terrestrial isoprene emissions using MEGAN (Model of
988 Emissions of Gases and Aerosols from Nature), Atmos. Chem. Phys.
989 Discuss., 6, 107–173, 2006.
990 Hack, J. J.: Parameterization of moist convection in the National Center for
991 Atmospheric Research community climate model (CCM2), J. Geophys.
992 Res., 99, 5551–5568, doi:10.1029/93jd03478, 1994.
993 He, Q., Li, C., Ma, J., Wang, H., Yan, X., Liang, Z., and Qi, G.: Enhancement of
994 aerosols in UTLS over the Tibetan Plateau induced by deep convection
995 during the Asian summer monsoon, Atmos. Chem. Phys. Discuss., 14,
996 3169-3191, 10.5194/acpd–14–3169–2014, 2014.
997 Hegde, P., Sudheer, A., Sarin, M., and Manjunatha, B.: Chemical
998 characteristics of atmospheric aerosols over southwest coast of India,
999 Atmos. Environ., 41, 7751–7766, 2007.
1000 Hofmann, D., Rosen, J., Harder, J., and Hereford, J.: Balloon-borne
1001 measurements of aerosol, condensation nuclei, and cloud particles in the
1002 stratosphere at McMurdo Station, Antarctica, during the spring of 1987, J.
1003 Geophys. Res., 94, 11253–11269, doi:10.1029/JD094iD09p11253, 1989.
1004 Huang, C., Chen, C. H., Li, L., Cheng, Z., Wang, H. L., Huang, H. Y., Streets, D.
1005 G., and Wang, Y. J.: Emission inventory of anthropogenic air pollutants
1006 and VOC species in the Yangtze River Delta region, China, Atmos. Chem.
1007 Phys., 11, 4105–4120, 2011.
1008 Huang, X., Song, Y., Li, M., Li, J., Huo, Q., Cai, X., Zhu, T., Hu, M., and Zhang,
1009 H.: A high-resolution ammonia emission inventory in China, Global
1010 Biogeochem. Cy., 26, GB1030, doi:10.1029/2011GB004161, 2012.
1011 Husain, L., Dutkiewicz, V. A., Khan, A., and Ghauri, B. M.: Characterization of
1012 carbonaceous aerosols in urban air, Atmos. Environ., 41, 6872–6883,
1013 2007.
1014 Jacob, D. J.: Heterogeneous chemistry and tropospheric ozone, Atmos.
1015 Environ., 34, 2131-2159, 2000.
1016 Jaeglé, L., Quinn, P., Bates, T., Alexander, B., and Lin, J.-T.: Global distribution
1017 of sea salt aerosols: new constraints from in situ and remote sensing
1018 observations, Atmos. Chem. Phys., 11, 3137–3157, 2011.
1019 Jayaraman, A., Gadhavi, H., Ganguly, D., Misra, A., Ramachandran, S., and
1020 Rajesh, T.: Spatial variations in aerosol characteristics and regional
1021 radiative forcing over India: Measurements and modeling of 2004 road
1022 campaign experiment, Atmos. Environ., 40, 6504–6515, 2006.

1023 Jeong, J. I., and Park, R. J.: Effects of the meteorological variability on regional
1024 air quality in East Asia, Atmos. Environ., 69, 46–55, 2013.
1025 Jiang, H., Liao, H., Pye, H., Wu, S., Mickley, L. J., Seinfeld, J. H., and Zhang,
1026 X.: Projected effect of 2000-2050 changes in climate and emissions on
1027 aerosol levels in China and associated transboundary transport, Atmos.
1028 Chem. Phys., 13, 7937–7960, 2013.
1029 Kar, J., Bremer, H., Drummond, J. R., Rochon, Y. J., Jones, D., Nichitiu, F., Zou,
1030 J., Liu, J., Gille, J. C., and Edwards, D. P.: Evidence of vertical transport of
1031 carbon monoxide from Measurements of Pollution in the Troposphere
1032 (MOPITT), Geophys. Res. Lett., 31, L23105, doi:10.1029/2004GL021128,
1033 2004.
1034 Kim, J., Song, C. H., Ghim, Y., Won, J., Yoon, S., Carmichael, G., and Woo, J.
1035 H.: An investigation on NH_3 emissions and particulate $NH_4^+ - NO_3^-$
1036 formation in East Asia, Atmos. Environ., 40, 2139–2150, 2006.
1037 Kim, Y.- S., Shibata, T., Iwasaka, Y., Shi, G., Zhou, X., Tamura, K., and Ohashi,
1038 T.: Enhancement of aerosols near the cold tropopause in summer over
1039 Tibetan Plateau: lidar and balloonborne measurements in 1999 at Lhasa,
1040 Tibet, China, in: Lidar Remote Sensing for Industry and Environment
1041 Monitoring III, edited by: Singh U. N., Itabe, T., and Liu, Z., Proceedings of
1042 SPIE, Hangzhou, China, 4893, 496–503, 2003.
1043 Kirner, O., Ruhnke, R., Buchholz-Dietsch, J., Jöckel, P., Brühl, C., and Steil, B.:
1044 Simulation of polar stratospheric clouds in the chemistry-climate-model
1045 EMAC via the submodel PSC, Geoscientific Model Development, 4, 169–
1046 182, 2011.
1047 Kulkarni, P., and Ramachandran, S.: Comparison of aerosol extinction
1048 between lidar and SAGE II over Gadanki, a tropical station in India, Ann.
1049 Geophys., 33, 3, 351–362, 2015.
1050 Kulshrestha, U., Saxena, A., Kumar, N., Kumari, K., and Srivastava, S.:
1051 Chemical composition and association of size-differentiated aerosols at a
1052 suburban site in a semi-arid tract of India, J. Atmos. Chem., 29, 109–118,
1053 1998.
1054 Latha, K. M., and Badarinath, K.: Seasonal variations of black carbon aerosols
1055 and total aerosol mass concentrations over urban environment in India,
1056 Atmos. Environ., 39, 4129–4141, 2005.
1057 Lau, K. M., Kim, M. K., and Kim, K. M.: Asian summer monsoon anomalies
1058 induced by aerosol direct forcing: the role of the Tibetan Plateau, Clim.
1059 Dyn., 26, 855–864, doi:10.1007/s00382-006-0114-z, 2006.
1060 Lawrence, M. G., and Lelieveld, J.: Atmospheric pollutant outflow from
1061 southern Asia: a review, Atmos. Chem. Phys., 10, 11017-11096,
1062 doi:10.5194/acp-10-11017-2010, 2010.
1063 Lelieveld, J., Crutzen, P. J., Ramanathan, V., Andreae, M. O., Brenninkmeijer,
1064 C. A. M., Campos, T., Cass, G. R., Dickerson, R. R., Fischer, H., de Gouw,
1065 J. A., Hansel, A., Jefferson, A., Kley, D., de Laat, A. T. J., Lal, S., Lawrence,
1066 M. G., Lobert, J. M., Mayol-Bracero, O. L., Mitra, A. P., Novakov, T.,
1067 Oltmans, S. J., Prather, K. A., Reiner, T., Rodhe, H., Scheeren, H. A.,
1068 Sikka, D., and Williams, J.: The Indian Ocean Experiment: Widespread air
1069 pollution from South and Southeast Asia, Science, 291, 1031–1036,
1070 doi:10.1126/science.1057103, 2001.
1071 Leon, J.-F., Chazette, P., Dulac, F., Pelon, J., Flamant, C., Bonazzola, M.,
1072 Foret, G., Alfaro, S., Cachier, H., and Cautenet, S.: Large-scale advection

of continental aerosols during INDOEX, J. Geophys. Res., 106, 28427–28428, 28439, 2001.
Li, Q., Jiang, J. H., Wu, D. L., Read, W. G., Livesey, N. J., Waters, J. W., Zhang, Y., Wang, B., Filipiak, M. J., and Davis, C. P.: Convective outflow of South Asian pollution: A global CTM simulation compared with EOS MLS observations, Geophys. Res. Lett., 32, L14826, doi:10.1029/2005GL022762, 2005.
Liao, H., Adams, P. J., Chung, S. H., Seinfeld, J. H., Mickley, L. J., and Jacob, D. J.: Interactions between tropospheric chemistry and aerosols in a unified general circulation model, J. Geophys. Res., 108, 4001, doi:10.1029/2001JD001260, 2003.
Liao, H., and Seinfeld, J. H.: Global impacts of gas-phase chemistry-aerosol interactions on direct radiative forcing by anthropogenic aerosols and ozone, J. Geophys. Res., 110, D18208, doi:10.1029/2005JD005907, 2005.
Liao, H., Zhang, Y., Chen, W.-T., Raes, F., and Seinfeld, J. H.: Effect of chemistry-aerosol-climate coupling on predictions of future climate and future levels of tropospheric ozone and aerosols, J. Geophys. Res., 114, D10306, doi:10.1029/2008JD010984, 2009.
Liu, H., Jacob, D. J., Bey, I., and Yantosca, R. M.: Constraints from 210Pb and 7Be on wet deposition and transport in a global three-dimensional chemical tracer model driven by assimilated meteorological fields, J. Geophys. Res., 106, 12109–12128, 2001.
Liu, X., Penner, J. E., and Wang, M.: Influence of anthropogenic sulfate and black carbon on upper tropospheric clouds in the NCAR CAM3 model coupled to the IMPACT global aerosol model, J. Geophys. Res., 114, D03204, doi:10.1029/2008JD010492, 2009.
Livesey, N. J., Filipiak, M. J., Froidevaux, L., Read, W. G., Lambert, A., Santee, M. L., Jiang, J. H., Pumphrey, H. C., Waters, J. W., and Cofield, R. E.: Validation of Aura Microwave Limb Sounder O_3 and CO observations in the upper troposphere and lower stratosphere, J. Geophys. Res., 113, D15S02, doi:10.1029/2007JD008805, 2008.
Livesey, N. J., Read, W. G., Wagner, P. A., Froidevaux, L., Lambert, A., Manney, G. L., Pumphrey, H. C., Santee, M. L., Schwartz, M. J., Wang, S., Cofield, R. E., Cuddy, D. T., Fuller, R. A., Jarnot, R. F., Jiang, J. H., and Knosp, B. W.: Version 3.3 Level 2 data quality and description document, JPL D-33509, 2011.
Lodhi, A., Ghauri, B., Khan, M. R., Rahman, S., and Shafique, S.: Particulate matter ($PM_{2.5}$) concentration and source apportionment in Lahore, J. Brazil. Chem. Soc., 20, 1811–1820, 2009.
Lou, S., Liao, H., and Zhu, B.: Impacts of aerosols on surface-layer ozone concentrations in China through heterogeneous reactions and changes in photolysis rates, Atmos. Environ., 85, 123–138, 2014.
Luo, Y., Zhang, R., Qian, W., Luo, Z., and Hu, X.: Inter-comparison of deep convection over the Tibetan Plateau–Asian monsoon region and subtropical North America in boreal summer using CloudSat/CALIPSO data, Journal of Climate, 24(8), 2164–2177, 2011.
Ma, J., Tang, J., Li, S.-M., and Jacobson, M. Z.: Size distributions of ionic aerosols measured at Waliguan Observatory: Implication for nitrate gas-to-particle transfer processes in the free troposphere, J. Geophys.

Res., 108, 4541, doi:10.1029/2002jd003356, 2003.
Martin, R. V., Jacob, D. J., Yantosca, R. M., Chin, M., and Ginoux, P.: Global and regional decreases in tropospheric oxidants from photochemical effects of aerosols, J. Geophys. Res., 108, 4097, doi:10.1029/2002JD002622, 2003.
Martin, R. V., Sauvage, B., Folkins, I., Sioris, C. E., Boone, C., Bernath, P., and Ziemke, J.: Space-based constraints on the production of nitric oxide by lightning, J. Geophys. Res., 112, D09309, doi:10.1029/2006JD007831, 2007.
McCormick, M. P.: SAGE II: an overview, Adv. Space Res., 7, 219-226, 1987.
McLinden, C., Olsen, S., Hannegan, B., Wild, O., Prather, M., and Sundet, J.: Stratospheric ozone in 3-D models: A simple chemistry and the cross-tropopause flux, J. Geophys. Res., 105, 14653–14665, doi:10.1029/2000JD900124, 2000.
Mickley, L. J., Murti, P., Jacob, D. J., Logan, J. A., Koch, D., and Rind, D.: Radiative forcing from tropospheric ozone calculated with a unified chemistry-climate model, J. Geophys. Res., 104, 30153-30172, 1999.
Ming, J., Zhang, D., Kang, S., and Tian, W.: Aerosol and fresh snow chemistry in the East Rongbuk Glacier on the northern slope of Mt. Qomolangma (Everest), J. Geophys. Res., 112, D15307, doi:10.1029/2007JD008618, 2007.
Momin, G. A., Rao, P. S. P., Safai, P. D., Ali, K., Naik, M. S., and Pillai, A. G.: Atmospheric aerosol characteristic studies at Pune and Thiruvananthapuram during INDOEX programme–1998, Curr. Sci., 76, 985-989, 1999.
Mu, Q., and Liao, H.: Simulation of the interannual variations of aerosols in China: role of variations in meteorological parameters, Atmos. Chem. Phys., 14, 9597–9612, 2014.
Murray, L. T., Jacob, D. J., Logan, J. A., Hudman, R. C., and Koshak, W. J.: Optimized regional and interannual variability of lightning in a global chemical transport model constrained by LIS/OTD satellite data, J. Geophys. Res., 117, D20307, doi:10.1029/2012JD017934, 2012.
Nair, P. R., George, S. K., Sunilkumar, S., Parameswaran, K., Jacob, S., and Abraham, A.: Chemical composition of aerosols over peninsular India during winter, Atmos. Environ., 40, 6477–6493, 2006.
Nair, V. S., Solmon, F., Giorgi, F., Mariotti, L., Babu, S. S., and Moorthy, K. K.: Simulation of South Asian aerosols for regional climate studies, J. Geophys. Res., 117, D04209, doi:10.1029/2011JD016711, 2012.
Nakamura, T., Matsumoto, K., and Uematsu, M.: Chemical characteristics of aerosols transported from Asia to the East China Sea: an evaluation of anthropogenic combined nitrogen deposition in autumn, Atmos. Environ., 39, 1749–1758, 2005.
Oberbeck, V. R., Livingston, J. M., Russell, P. B., Pueschel, R. F., Rosen, J. N., Osborn, M. T., Kritz, M. A., Snetsinger, K. G., and Ferry, G. V.: SAGE II aerosol validation: Selected altitude measurements, including particle micromeasurements, J. Geophys. Res., 94, 8367–8380, doi:10.1029/JD094iD06p08367, 1989.
Pant, P., Hegde, P., Dumka, U., Sagar, R., Satheesh, S., Moorthy, K. K., Saha, A., and Srivastava, M.: Aerosol characteristics at a high-altitude location in central Himalayas: Optical properties and radiative forcing, J. Geophys.

Res., 111, D17206, doi:10.1029/2005JD006768, 2006.
Park, M., Randel, W. J., Kinnison, D. E., Garcia, R. R., and Choi, W.: Seasonal variation of methane, water vapor, and nitrogen oxides near the tropopause: Satellite observations and model simulations, J. Geophys. Res., 109, D03302, doi:10.1029/2003JD003706, 2004.
Park, M., Randel, W. J., Gettelman, A., Massie, S. T., and Jiang, J. H.: Transport above the Asian summer monsoon anticyclone inferred from Aura Microwave Limb Sounder tracers, J. Geophys. Res., 112, D16309, doi:10.1029/2006JD008294, 2007.
Park, M., Randel, W. J., Emmons, L. K., Bernath, P. F., Walker, K. A., and Boone, C. D.: Chemical isolation in the Asian monsoon anticyclone observed in Atmospheric Chemistry Experiment (ACE–FTS) data, Atmos. Chem. Phys., 8, 757–764, 2008.
Park, M., Randel, W. J., Emmons, L. K., and Livesey, N. J.: Transport pathways of carbon monoxide in the Asian summer monsoon diagnosed from Model of Ozone and Related Tracers (MOZART), J. Geophys. Res., 114, D08303, doi:10.1029/2008JD010621, 2009.
Park, R. J., Jacob, D. J., Chin, M., and Martin, R. V.: Sources of carbonaceous aerosols over the United States and implications for natural visibility, J. Geophys. Res., 108, 4355, doi:10.1029/2002JD003190, 2003.
Park, R. J., Jacob, D. J., Field, B. D., Yantosca, R. M., and Chin, M.: Natural and transboundary pollution influences on sulfate–nitrate–ammonium aerosols in the United States: Implications for policy, J. Geophys. Res., 109, D15204, doi:10.1029/2003JD004473, 2004.
Pitari, G., Aquila, V., Kravitz, B., Robock, A., Watanabe, S., Cionni, I., Luca, N. D., Genova, G. D., Mancini, E., and Tilmes, S.: Stratospheric ozone response to sulfate geoengineering: Results from the Geoengineering Model Intercomparison Project (GeoMIP), J. Geophys. Res., 119, 2629–2653, doi: 10.1002/2013JD020566, 2014.
Pitari, G., Iachetti, D., Genova, G. D., De Luca, N., Søvde, O., Hodnebrog, Ø., Lee, D. S., and Lim, L. L.: Impact of coupled NO_x/aerosol aircraft emissions on ozone photochemistry and radiative forcing, Atmosphere,6, 751–782, doi:10.3390/atmos6060751, 2015.
Popp, P., Marcy, T., Jensen, E., Kärcher, B., Fahey, D., Gao, R., Thompson, T., Rosenlof, K., Richard, E., and Herman, R.: The observation of nitric acid-containing particles in the tropical lower stratosphere, Atmos. Chem. Phys., 6, 601-611, 2006.
Pye, H., Liao, H., Wu, S., Mickley, L. J., Jacob, D. J., Henze, D. K., and Seinfeld, J.: Effect of changes in climate and emissions on future sulfate–nitrate–ammonium aerosol levels in the United States, J. Geophys. Res., 114, D01205, doi:10.1029/2008JD010701, 2009.
Qie, X., Wu, X., Yuan, T., Bian, J., and Lü, D.: Comprehensive Pattern of Deep Convective Systems over the Tibetan Plateau–South Asian Monsoon Region Based on TRMM Data, J. Clim., 27, 6612–6626, 2014.
Ram, K., Sarin, M., and Hegde, P.: Atmospheric abundances of primary and secondary carbonaceous species at two high-altitude sites in India: Sources and temporal variability, Atmos. Environ., 42, 6785-6796, 2008.
Ramanathan, V., Li, F., Ramana, M., Praveen, P., Kim, D., Corrigan, C., Nguyen, H., Stone, E. A., Schauer, J. J., and Carmichael, G.: Atmospheric brown clouds: Hemispherical and regional variations in long-range

transport, absorption, and radiative forcing, J. Geophys. Res., 112, D22S21, doi:10.1029/2006JD008124, 2007.
Randel, W. J., and Park, M.: Deep convective influence on the Asian summer monsoon anticyclone and associated tracer variability observed with Atmospheric Infrared Sounder (AIRS), J. Geophys. Res., 111, D12314, doi:10.1029/2005JD006490, 2006.
Randel, W. J., Park, M., Emmons, L., Kinnison, D., Bernath, P., Walker, K. A., Boone, C., and Pumphrey, H.: Asian monsoon transport of pollution to the stratosphere, Science, 328, 611–613, 2010.
Rasch, P. J., Tilmes, S., Turco, R. P., Robock, A., Oman, L., Chen, C. C., Stenchikov, G. L., and Garcia, R. R.: An overview of geoengineering of climate using stratospheric sulphate aerosols, Philos. Trans. R. Soc. A-Math. Phys. Eng. Sci., 366, 4007-4037, doi:10.1098/rsta.2008.0131, 2008.
Rastogi, N., and Sarin, M.: Long-term characterization of ionic species in aerosols from urban and high-altitude sites in western India: Role of mineral dust and anthropogenic sources, Atmos. Environ., 39, 5541–5554, 2005.
Rastogi, N., and Sarin, M.: Quantitative chemical composition and characteristics of aerosols over western India: one-year record of temporal variability, Atmos. Environ., 43, 3481–3488, 2009.
Rengarajan, R., Sarin, M., and Sudheer, A.: Carbonaceous and inorganic species in atmospheric aerosols during wintertime over urban and high-altitude sites in North India, J. Geophys. Res., 112, D21307, doi:10.1029/2006JD008150, 2007.
Russell, P. B., and Mccormick, M. P.: SAGE II aerosol data validation and initial data use: An introduction and overview, J. Geophys. Res., 94, 8335–8338, 1989.
Safai, P., Kewat, S., Praveen, P., Rao, P., Momin, G., Ali, K., and Devara, P.: Seasonal variation of black carbon aerosols over a tropical urban city of Pune, India, Atmos. Environ., 41, 2699–2709, 2007.
Salam, A., Bauer, H., Kassin, K., Mohammad Ullah, S., and Puxbaum, H.: Aerosol chemical characteristics of a mega-city in Southeast Asia (Dhaka–Bangladesh), Atmos. Environ., 37, 2517–2528, 2003.
Santee, M., Lambert, A., Read, W., Livesey, N., Cofield, R., Cuddy, D., Daffer, W., Drouin, B., Froidevaux, L., and Fuller, R.: Validation of the Aura Microwave Limb Sounder HNO_3 measurements, J. Geophys. Res., 112, D24S40, doi:10.1029/2007JD008721, 2007.
Sauvage, B., Martin, R., Donkelaar, A. v., Liu, X., Chance, K., Jaeglé, L., Palmer, P., Wu, S., and Fu, T.-M.: Remote sensed and in situ constraints on processes affecting tropical tropospheric ozone, Atmos. Chem. Phys., 7, 815–838, 2007.
Seinfeld, J. H., and Pandis, S. N.: Atmospheric chemistry and physics: from air pollution to climate change, second ed. John Wiley: A Wiley-Interscience Publication Press, 2006.
Sharma, R. K., Bhattarai, B., Sapkota, B., Gewali, M., and Kjeldstad, B.: Black carbon aerosols variation in Kathmandu valley, Nepal, Atmos. Environ., 63, 282–288, doi:10.1016/j.atmosenv.2012.09.023, 2012.
Shrestha, A. B., Wake, C. P., Dibb, J. E., Mayewski, P. A., Whitlow, S. I., Carmichael, G. R., and Ferm, M.: Seasonal variations in aerosol

concentrations and compositions in the Nepal Himalaya, Atmos. Environ., 34, 3349–3363, 10.1016/s1352-2310(99)00366-0, 2000.

Škerlak, B., Sprenger, M., and Wernli, H.: A global climatology of stratosphere-troposphere exchange using the ERA-Interim data set from 1979 to 2011, Atmos. Chem. Phys, 14, 913–937, 2014.

Stevenson, D. S., Dentener, F. J., Schultz, M. G., Ellingsen, K., Van Noije, T. P. C., Wild, O., Zeng, G., Amann, M., Atherton, C. S., and Bell, N.: Multimodel ensemble simulations of present-day and near-future tropospheric ozone, J. Geophys. Res., 111, D08301, doi:10.1029/2005JD006338, 2006.

Streets, D. G., Bond, T. C., Carmichael, G. R., Fernandes, S. D., Fu, Q., He, D., Klimont, Z., Nelson, S. M., Tsai, N. Y., and Wang, M. Q.: An inventory of gaseous and primary aerosol emissions in Asia in the year 2000, J. Geophys. Res., 108, GTE 30–31, 2003.

Su, H., Jiang, J. H., Lu, X. H., Penner, J. E., Read, W. G., Massie, S., Schoeberl, M. R., Colarco, P., Livesey, N. J., and Santee, M. L.: Observed Increase of TTL Temperature and Water Vapor in Polluted Clouds over Asia, J. Clim., 24, 2728–2736, 10.1175/2010jcli3749.1, 2011.

Sudheer, A., and Sarin, M.: Carbonaceous aerosols in MABL of Bay of Bengal: Influence of continental outflow, Atmos. Environ., 42, 4089-4100, 2008.

Talukdar, R. K., Burkholder, J. B., Roberts, J. M., Portmann, R. W., and Ravishankara, A.: Heterogeneous Interaction of N_2O_5 with HCl Doped H_2SO_4 under Stratospheric Conditions: $ClNO_2$ and Cl_2 Yields, J. Phys. Chem. A., 116, 6003–6014, 2012.

Tang, M., Telford, P., Pope, F., Rkiouak, L., Abraham, N., Archibald, A., Braesicke, P., Pyle, J., McGregor, J., and Watson, I.: Heterogeneous reaction of N_2O_5 with airborne TiO_2 particles and its implication for stratospheric particle injection, Atmos. Chem. Phys., 14, 6035–6048, 2014.

Tare, V., Tripathi, S., Chinnam, N., Srivastava, A., Dey, S., Manar, M., Kanawade, V. P., Agarwal, A., Kishore, S., and Lal, R.: Measurements of atmospheric parameters during Indian Space Research Organization Geosphere Biosphere Program Land Campaign II at a typical location in the Ganga Basin: 2. chemical properties, J. Geophys. Res., 111, D23210, doi:10.1029/2006JD007279, 2006.

Thornton, J. A., Jaeglé, L., and McNeill, V. F.: Assessing known pathways for HO_2 loss in aqueous atmospheric aerosols: Regional and global impacts on tropospheric oxidants, J. Geophys. Res., 113, D05303, doi:10.1029/2007JD009236, 2008.

Tobo, Y., Zhang, D., Iwasaka, Y., and Shi, G.: On the mixture of aerosols and ice clouds over the Tibetan Plateau: Results of a balloon flight in the summer of 1999, Geophys. Res. Lett., 34, L23801, doi:10.1029/2007GL031132, 2007.

Tripathi, S., Dey, S., Tare, V., and Satheesh, S.: Aerosol black carbon radiative forcing at an industrial city in northern India, Geophys. Res. Lett., 32, L08802, doi:10.1029/2005GL022515, 2005.

van der Werf, G. R., Randerson, J. T., Giglio, L., Collatz, G. J., Mu, M., Kasibhatla, P. S., Morton, D. C., DeFries, R. S., Jin, Y., and van Leeuwen, T. T.: Global fire emissions and the contribution of deforestation, savanna, forest, agricultural, and peat fires (1997–2009), Atmos. Chem. Phys., 10,

11707–11735, 2010.
Vanhellemont, F., Tetard, C., Bourassa, A., Fromm, M., Dodion, J., Fussen, D., Brogniez, C., Degenstein, D., Gilbert, K., and Turnbull, D.: Aerosol extinction profiles at 525 nm and 1020 nm derived from ACE imager data: comparisons with GOMOS, SAGE II, SAGE III, POAM III, and OSIRIS, Atmos. Chem. Phys., 8, 2027-2037, 2008.
Venkataraman, C., Reddy, C. K., Josson, S., and Reddy, M. S.: Aerosol size and chemical characteristics at Mumbai, India, during the INDOEX-IFP (1999), Atmos. Environ., 36, 1979–1991, 2002.
Verma, S., Boucher, O., Reddy, M., Upadhyaya, H., Van, P., Binkowski, F., and Sharma, O.: Tropospheric distribution of sulphate aerosols mass and number concentration during INDOEX-IFP and its transport over the Indian Ocean: a GCM study, Atmos. Chem. Phys., 12, 6185–6196, 2012.
Vernier, J.-P., Pommereau, J.-P., Garnier, A., Pelon, J., Larsen, N., Nielsen, J., Christensen, T., Cairo, F., Thomason, L., and Leblanc, T.: Tropical stratospheric aerosol layer from CALIPSO lidar observations, J. Geophys. Res., 114, D00H10, doi:10.1029/2009JD011946, 2009.
Vernier, J. P., Thomason, L., and Kar, J.: CALIPSO detection of an Asian tropopause aerosol layer, Geophys. Res. Lett., 38, L07804, doi:10.1029/2010GL046614, 2011.
Voigt, C., Schreiner, J., Kohlmann, A., Zink, P., Mauersberger, K., Larsen, N., Deshler, T., Kröger, C., Rosen, J., and Adriani, A.: Nitric acid trihydrate (NAT) in polar stratospheric clouds, Science, 290, 1756-1758, 2000.
Wang, P., McCormick, M., McMaster, L., Chu, W., Swissler, T., Osborn, M., Russell, P., Oberbeck, V., Livingston, J., and Rosen, J.: SAGE II aerosol data validation based on retrieved aerosol model size distribution from SAGE II aerosol measurements, J. Geophys. Res., 94, 8381–8393, doi:10.1029/JD094iD06p08381, 1989.
Wang, Y., Logan, J. A., and Jacob, D. J.: Global simulation of tropospheric O_3–NO_x–hydrocarbon chemistry: 2. Model evaluation and global ozone budget, J. Geophys. Res., 103, 10727–10755, 1998.
Wang, Y., Zhang, Q., He, K., Zhang, Q., and Chai, L.: Sulfate-nitrate-ammonium aerosols over China: response to 2000–2015 emission changes of sulfur dioxide, nitrogen oxides, and ammonia, Atmos. Chem. Phys., 13, 2635–2652, 2013.
Waters, J. W., Froidevaux, L., Harwood, R. S., Jarnot, R. F., Pickett, H. M., Read, W. G., Siegel, P. H., Cofield, R. E., Filipiak, M. J., and Flower, D.: The earth observing system microwave limb sounder (EOS MLS) on the Aura satellite, IEEE T. Geosci. Remote., 44, 1075-1092, 2006.
Weigel, R., Borrmann, S., Kazil, J., Minikin, A., Stohl, A., Wilson, J., Reeves, J., Kunkel, D., De Reus, M., and Frey, W.: In situ observations of new particle formation in the tropical upper troposphere: the role of clouds and the nucleation mechanism, Atmos. Chem. Phys. Discuss., 11, 2011.
Wesely, M.: Parameterization of surface resistances to gaseous dry deposition in regional-scale numerical models, Atmos. Environ., 23, 1293-1304, 1989.
Wu, L. T., Su, H., and Jiang, J. H.: Regional simulations of deep convection and biomass burning over South America: 2. Biomass burning aerosol effects on clouds and precipitation, J. Geophys. Res., 116, doi:10.1029/2011jd01 6106, 2011.

1373 Wu, S., Mickley, L. J., Jacob, D. J., Logan, J. A., Yantosca, R. M., and Rind, D.:
1374 Why are there large differences between models in global budgets of
1375 tropospheric ozone? J. Geophys. Res., 112, D05302,
1376 doi:10.1029/2006JD007801, 2007.
1377 Wu, S., Mickley, L. J., Jacob, D. J., Rind, D., and Streets, D. G.: Effects of
1378 2000–2050 changes in climate and emissions on global tropospheric
1379 ozone and the policy–relevant background surface ozone in the United
1380 States, J. Geophys. Res., 113, D18312, doi:10.1029/2007JD009639,
1381 2008.
1382 Xia, X., Zong, X., Cong, Z., Chen, H., Kang, S., and Wang, P.: Baseline
1383 continental aerosol over the central Tibetan plateau and a case study of
1384 aerosol transport from South Asia, Atmos. Environ., 45, 7370-7378, 2011.
1385 Xiong, X., Houweling, S., Wei, J., Maddy, E., Sun, F., and Barnet, C.: Methane
1386 plume over south Asia during the monsoon season: satellite observation
1387 and model simulation, Atmos. Chem. Phys., 9, 783-794, 2009.
1388 Yanai, M., Li, C., and Song, Z.: Seasonal heating of the Tibetan Plateau and its
1389 effects on the evolution of the Asian summer monsoon, J. Meteorol. Soc.
1390 Jan., 70, 319–351, 1992.
1391 Yao, X., Chan, C. K., Fang, M., Cadle, S., Chan, T., Mulawa, P., He, K., and Ye,
1392 B.: The water-soluble ionic composition of $PM_{2.5}$ in Shanghai and Beijing,
1393 China, Atmos. Environ., 36, 4223–4234, 2002.
1394 Yin, Y., Chen, Q., Jin, L., Chen, B., Zhu, S., and Zhang, X.: The effects of deep
1395 convection on the concentration and size distribution of aerosol particles
1396 within the upper troposphere: A case study, J. Geophys. Res., 117,
1397 D22202, doi:10.1029/2012JD017827, 2012.
1398 Zeng, G., Pyle, J., and Young, P.: Impact of climate change on tropospheric
1399 ozone and its global budgets, Atmos. Chem. Phys., 8, 369-387, 2008.
1400 Zhang, G. J., and McFarlane, N. A.: Sensitivity of climate simulations to the
1401 parameterization of cumulus convection in the Canadian Climate Centre
1402 general circulation model, Atmos.-Ocean, 33, 407–446, 1995.
1403 Zhang, L., Liao, H., and Li, J.: Impacts of Asian summer monsoon on seasonal
1404 and interannual variations of aerosols over eastern China, J. Geophys.
1405 Res., 115, D00K05, doi:10.1029/2009JD012299, 2010.
1406 Zhang, N., Cao, J., Ho, K., and He, Y.: Chemical characterization of aerosol
1407 collected at Mt. Yulong in wintertime on the southeastern Tibetan Plateau,
1408 Atmos. Res., 107, 76, 2012.
1409 Zhang, Q., Streets, D. G., Carmichael, G. R., He, K., Huo, H., Kannari, A.,
1410 Klimont, Z., Park, I., Reddy, S., and Fu, J.: Asian emissions in 2006 for the
1411 NASA INTEX-B mission, Atmos. Chem. Phys., 9, 5131–5153, 2009.
1412 Zhang, X., Cao, J., Li, L., Arimoto, R., Cheng, Y., Huebert, B., and Wang, D.:
1413 Characterization of atmospheric aerosol over Xian in the south margin of
1414 the Loess Plateau, China, Atmos. Environ., 36, 4189–4199, 2002.
1415 Zhang, Y., Dore, A., Ma, L., Liu, X., Ma, W., Cape, J., and Zhang, F.:
1416 Agricultural ammonia emissions inventory and spatial distribution in the
1417 North China Plain, Environ. Pollut., 158, 490–501, 2010.
1418 Zhao, X., Turco, R. P., Kao, C. Y. J., and Elliott, S.: Aerosol-induced chemical
1419 perturbations of stratospheric ozone: Three-dimensional simulations and
1420 analysis of mechanisms, J. Geophys. Res., 102, 3617–3637,
1421 doi:10.1029/96jd03406, 1997.
1422 Zhu, J., Liao, H., and Li, J.: Increases in aerosol concentrations over

1423 eastern China due to the decadal-scale weakening of the East Asian
1424 summer monsoon, Geophys. Res. Lett., 39, L09809,
1425 doi:10.1029/2012GL051428, 2012.

1426 Table 1. Summary of Annual Emissions of Aerosols and Aerosol
1427 Precursors in Asia (60°E-155°E, 10°N-55°N)

Species	Global	Asia
NO_x (Tg N yr^{-1})		
Aircraft	0.5	0.08
Anthropogenic	28.6	9.96
Biomass burning	4.7	0.27
Fertilizer	0.7	0.31
Lightning	5.9	0.87
Soil	5.9	0.96
Total	46.3	12.45
SO_2 (Tg S yr^{-1})		
Aircraft	0.1	0.01
Anthropogenic	52.6	23.46
Biomass burning	1.2	0.07
Volcanoes	4.4	1.04
No_eruption	8.9	1.78
Ship	7.4	0.94
Total	74.6	27.30
NH_3 (Tg N yr^{-1})		
Anthropogenic	34.9	17.83
Natural	14.2	2.01
Biomass burning	3.5	0.21
Biofuel	1.6	0.71
Total	54.2	20.76
OC (Tg C yr^{-1})		
Anthropogenic	3.1	1.42
Biomass burning	18.7	1.10
Biofuel	6.3	3.28
Biogenic	9.7	1.22
Total	37.8	7.02
BC (Tg C yr^{-1})		
Anthropogenic	3.0	1.43
Biomass burning	2.2	0.12
Biofuel	1.6	0.86
Total	6.8	2.41

Table 2. Simulated seasonal mean concentrations of aerosols and their contributions to $PM_{2.5}$ (in percentages in parentheses) during summertime (June-August) of 2005 for the TP/SASM, TP, and SASM regions. The unit is μg m^{-3} for concentrations at the surface, and 10^{-2} μg m^{-3} for concentrations at 200 hPa and 100 hPa.

	$PM_{2.5}$	SO_4^{2-}	NO_3^-	NH_4^+	OC	BC
			TP/SASM			
Surface	4.73	1.70(35.9%)	0.94(19.8%)	0.85(18.1%)	0.94(19.8%)	0.30(6.4%)
200 hPa	16.19	3.27(20.2%)	7.57(46.8%)	2.67(16.5%)	2.22(13.7%)	0.44(2.7%)
100 hPa	12.14	2.60(21.4%)	6.90(56.8%)	1.43(11.8%)	1.05(8.6%)	0.16(1.3%)
			TP			
Surface	5.44	2.12(39.0%)	1.05(19.3%)	1.08(19.9%)	0.88(16.1%)	0.31(5.7%)
200 hPa	19.80	4.16(21.0%)	9.43(47.6%)	3.25(16.4%)	2.49(12.6%)	0.47(2.4%)
100 hPa	10.58	2.60(24.6%)	5.51(52.0%)	1.35(12.7%)	0.99(9.4%)	0.14(1.3%)
			SASM			
Surface	4.02	1.28(31.8%)	0.83(20.5%)	0.63(15.6%)	1.00(24.8%)	0.29(7.2%)
200 hPa	12.57	2.38(18.9%)	5.72(45.5%)	2.10(16.7%)	1.95(15.5%)	0.41(3.3%)
100 hPa	13.71	2.60(19.0%)	8.30(60.5%)	1.52(11.1%)	1.11(8.1%)	0.18(1.3%)

Table 3. List of gas-phase reactions and heterogeneous reactions involve HNO_3 in the GEOS-Chem model (Version 9-01-03)

	Reactants		Products
	Chemical productions		
R1	$NO_2 + OH + M$	→	$HNO_3 + M$
R2	$NO_3 + CH_2O$	→	HNO_3 + prod.
R3	$ALD_2 + NO_3$	→	HNO_3 + prod.
R4	$RIO_1 + NO$	→	HNO_3 + prod.
R5	$IAO_2 + NO$	→	$0.08HNO_3$+ prod.
R6	$ISN_1 + NO$	→	$0.05HNO_3$ + prod.
R7	$VRO_2 + NO$	→	HNO_3 + prod.
R8	$MRO_2 + NO$	→	HNO_3 + prod.
R9	INO_2+NO	→	$0.85HNO_3$+ prod.
R10	$ALK_4 + NO_3$	→	HNO_3 + prod.
R11	$RCHO + NO_3$	→	HNO_3 + prod.
R12	$MEK + NO_3$	→	HNO_3 + prod.
R13	$INO_2 + MO_2$	→	$0.425HNO_3$ + prod.
R14	$GLYX + NO_3$	→	HNO_3 + prod.
R15	$MGLY + NO_3$	→	HNO_3 + prod.
R16	$MACR + NO_3$	→	HNO_3 + prod.
R17	$C_2H_6 + NO_3$	→	HNO_3 + prod
R18	$INO_2 + MCO_3$	→	$0.85HNO_3$ + prod.
R19	NO_2 + (aerosol)	→	$0.5HNO_3$+ prod.
R20	NO_3 + (aerosol)	→	HNO_3 + prod.
R21	N_2O_5 + (aerosol)	→	$2HNO_3$
R22	$DMS + NO_3$	→	HNO_3 + prod.
R23	$BrNO_3 + H_2O$(l,s)	→	HNO_3 + prod.
	Chemical loss		
R24	$HNO_3 + OH$	→	$H_2O + NO_3$
R25	HNO_3 + hv	→	$OH + NO_2$

Table 4. Sensitivity simulations to examine the impacts of uncertainties in surface-layer aerosol concentrations on simulated NO_3^- in the UTLS. "Conc" and "Ctri" denote, respectively, simulated seasonal mean concentrations of SO_4^{2-}, NO_3^-, NH_4^+, OC, BC and their contributions to $PM_{2.5}$ (in percentages) during summertime (June-August) of 2005. The mass concentrations are averaged over the TP/SASM region, with unit of μg m^{-3} at the surface layer and of 10^{-2} μg m^{-3} at 200 hPa and 100 hPa. Also shown are the NMBs, as the simulated surface-layer concentrations are compared with measurements described in Section 4.2.

Species	Baseline Case			SO_2 (+20%)			NO_x (-50%)			NH_3 (-50%)			All Change		
	Conc.	Ctri.	NMB	Conc.	Ctri.	NMB	Conc.	Ctri.	NMB	Conc.	Ctri.	NMB	Conc.	Ctri.	NMB
Surface															
SO_4^{2-}	1.70	35.9%	–14.7%	1.92	38.1%	–4.4%	1.58	39.5%	–18.1%	1.70	38.1%	–14.7%	1.78	43.2%	–8.3%
NO_3^-	0.94	19.8%	+51.5%	0.94	18.7%	+53.5%	0.50	12.5%	–11.7%	0.73	16.4%	+24.1%	0.39	9.5%	–27.0%
NH_4^+	0.85	18.1%	+74.9%	0.94	18.6%	+93.8%	0.68	17.1%	+44.1%	0.78	17.6%	+64.6%	0.71	17.3%	+55.4%
OC	0.94	19.8%	–57.2%	0.94	18.6%	–57.2%	0.94	23.4%	–57.2%	0.94	21.0%	–57.2%	0.94	22.7%	–57.2%
BC	0.30	6.4%	–32.2%	0.30	6.0%	–32.2%	0.30	7.5%	–32.2%	0.30	6.8%	–32.2%	0.30	7.3%	–32.2%
200 hPa															
SO_4^{2-}	3.27	20.2%		3.67	22.9%		3.31	20.6%		3.29	29.1%		3.74	33.7%	
NO_3^-	7.57	46.8%		7.05	43.9%		7.41	46.0%		3.86	34.2%		3.19	28.7%	
NH_4^+	2.67	16.5%		2.67	16.6%		2.71	16.8%		1.49	13.2%		1.50	13.5%	
OC	2.22	13.7%		2.22	13.8%		2.22	13.8%		2.22	19.7%		2.22	20.0%	
BC	0.44	2.7%		0.44	2.7%		0.44	2.7%		0.44	3.9%		0.44	4.0%	
100 hPa															
SO_4^{2-}	2.60	21.4%		2.80	23.0%		2.66	21.9%		2.60	25.2%		2.87	27.2%	
NO_3^-	6.90	56.8%		6.72	55.3%		6.81	56.1%		5.68	55.0%		5.62	53.3%	
NH_4^+	1.43	11.8%		1.43	11.7%		1.45	12.0%		0.84	8.1%		0.84	8.0%	
OC	1.05	8.6%		1.05	8.6%		1.05	8.7%		1.05	10.2%		1.05	10.0%	
BC	0.16	1.3%		0.16	1.3%		0.16	1.3%		0.16	1.6%		0.16	1.5%	

Figure Captions

Figure. 1. Regions examined in this study: the Tibetan Plateau region (TP, 70–105°E, 25–40°N), the SASM region (SASM, 70–105°E, 10–25°N), and the anticyclone region of (20–120°E, 10–40°N).

Figure. 2. Monthly variations in emissions of NO_x (Tg N month^{-1}), SO_2 (Tg S month^{-1}), NH_3 (Tg N month^{-1}), OC (Tg C month^{-1}), and BC (Tg C month^{-1}) over Asia. Values shown are the total emissions (anthropogenic plus natural emissions listed in Table 1).

Figure. 3. Simulated global distributions of surface-layer HNO_3 (pptv) and O_3 (ppbv) averaged over June-August, 2005.

Figure. 4. Comparisons of simulated HNO_3 concentrations (pptv) with observations (pptv) from MLS. (a) and (b) are simulated concentrations at 200 hPa and 100 hPa, respectively. (c) is the latitude-altitude cross section of simulated HNO_3 concentrations averaged over 70–105°E. (d)-(f) are the same as (a)-(c), except that (d)-(f) are observations from MLS. The GEOS-Chem HNO_3 simulations are smoothed by the corresponding averaging kernels (AK). White areas indicate lack of data meeting the retrieval quality criteria. All the data are averaged over June-August of 2005.

Figure. 5. Comparisons of simulated O_3 concentrations (ppbv) with observations (ppbv) from MLS. (a) and (b) are simulated concentrations at 200 hPa and 100 hPa, respectively. (c) is the latitude-altitude cross section of simulated O_3 concentrations averaged over 70–105°E. (d)-(f) are the same as (a)-(c), except that (d)-(f) are observations from MLS. The GEOS-Chem O_3 simulations are smoothed by the corresponding averaging kernels. White areas indicate lack of data meeting the retrieval quality criteria. All the data are averaged over June-August of 2005.

Figure. 6. The simulated and observed vertical profiles of monthly mean O_3 mixing ratios at (a) Kunming and (b) Lhasa in August. The model results are from the simulation of year 2005. The observations in Kunming were conducted during August 7–13 (11 profiles of O_3 collected) in 2009 and during August 12–31 in 2012 (daily observations). The observations in Lhasa were conducted during August 22–28 in 2010 (12 profiles of O_3 collected) and during August 4–26 in 2013 (daily observations).

Figure. 7. Simulated seasonal mean concentrations (μg m^{-3}) of sulfate, nitrate, ammonium, organic carbon, black carbon, and $PM_{2.5}$ (defined as the sum of sulfate, nitrate, ammonium, BC, and OC) at (a) the surface layer, (b) 200 hPa, and (c) 100 hPa, during summer (June-August) of year 2005. Note that color bars are different for concentrations at the surface, 200 hPa, and 100 hPa.

Figure. 8. (a) Locations with measured aerosol concentrations from previous studies. Also shown are surface winds during summertime. (b)–(f) show the comparisons of simulated seasonal mean concentrations of sulfate, nitrate,

ammonium, OC, and BC with measured values, respectively. Also shown in (b)–(f) are the 1:1 line (dashed), linear fit (solid line and equation), correlation coefficient between simulated and measured concentrations (R), and normalized mean bias (NMB) (defined as NMB=$\frac{\sum_{i=1}^{n}(P_i-O_i)}{\sum_{i=1}^{n}O_i}$ ×100%, where P_i and O_i are predicted and observed concentrations at station *i* for each aerosol species).

Figure. 9. (a) Monthly mean distribution of aerosol extinction coefficients (km^{-1}) at 100 hPa for July of 2005. (b) Monthly mean vertical distributions of aerosol extinction coefficients (at 525 nm for SAGE II and 550 nm for GEOS-Chem, with the contributions of both anthropogenic and natural aerosols considered) (km^{-1}) averaged over the Asian monsoon anticyclone region (20–120°E, 10–40°N) for July of 2005. The horizontal dashed line represents the tropopause averaged over the Asian monsoon anticyclone region simulated by the GEOS-Chem model.

Figure. 10. Simulated contributions of nitrate to $PM_{2.5}$ (C_{NIT}= [NIT]/ [$PM_{2.5}$] ×100%) averaged over summer (June-August) of year 2005 at (a) surface-layer, (b) 200 hPa, and (c) 100 hPa. (d) The latitude-altitude cross section of simulated C_{NIT} (%) averaged over 70–105°E.

Figure. 11. Latitude-altitude cross sections of simulated concentrations (color shades, μg m^{-3}) of SO_4^{2-} and NO_3^- averaged over 70–105°E in June-August of 2005, together with the wind vectors obtained from the European Centre for Medium-Range Weather Forecasts (ECMWF) ERA-Interim Reanalysis data. The black line is the tropopause simulated by the GEOS-Chem model.

Figure. 12. Profiles of the net chemical production of HNO_3 by gas-phase reactions and heterogeneous reactions (red dotted line), the production of nitrate from gas to aerosol conversion of HNO_3 (blue dotted line) and the transport contributions of HNO_3 over the TP/SASM (70–105°E, 10–40°N). Also shown is the average HNO_3 mixing ratios (black dotted line) over the TP/SASM region during summertime of year 2005.

Figure. 13. (a)-(b) Distributions of RH (%) and temperature (K) at 100 hPa. (c)-(d) The latitude-altitude cross sections of RH (%) and temperature (K) averaged over 70–105°E. RH and temperature are from the GEOS5 assimilated meteorological fields, and all the values are the averages over June-August of year 2005.

Figure. 14. Mass budget for nitrate aerosol within the selected box of (70–105°E, 10–40°N, 8–16 km). E/W transport indicates net mass flux through the east and west lateral boundaries, N/S transport indicates net mass flux through the north and south lateral boundaries, and upward transport is the net mass flux through the top and bottom sides of the box. The mass flux is positive if it increases nitrate mass within the box. Unit of fluxes is Tg $season^{-1}$. All the values are the averages over June-August of 2005.

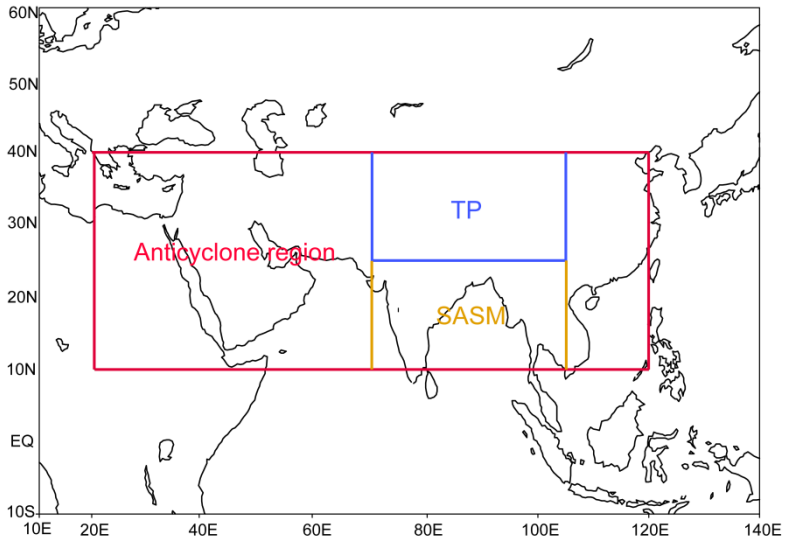

Figure. 1. Regions examined in this study: the Tibetan Plateau region (TP, 70–105°E, 25–40°N), the SASM region (SASM, 70–105°E, 10–25°N), and the anticyclone region of (20–120°E, 10–40°N).

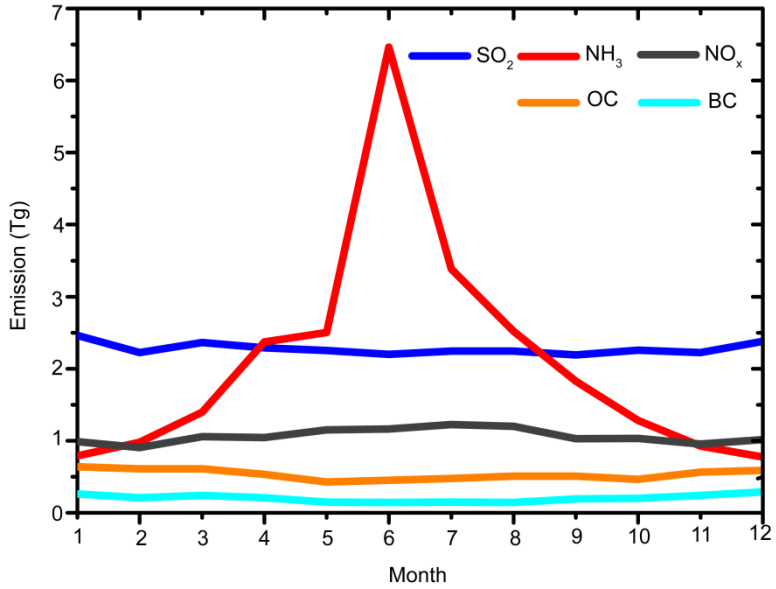

Figure. 2. Monthly variations in emissions of NO_x (Tg N month $^{-1}$), SO_2 (Tg S month^{-1}), NH_3 (Tg N month $^{-1}$), OC (Tg C month $^{-1}$), and BC (Tg C month $^{-1}$) over Asia. Values shown are the total emissions (anthropogenic plus natural emissions listed in Table 1).

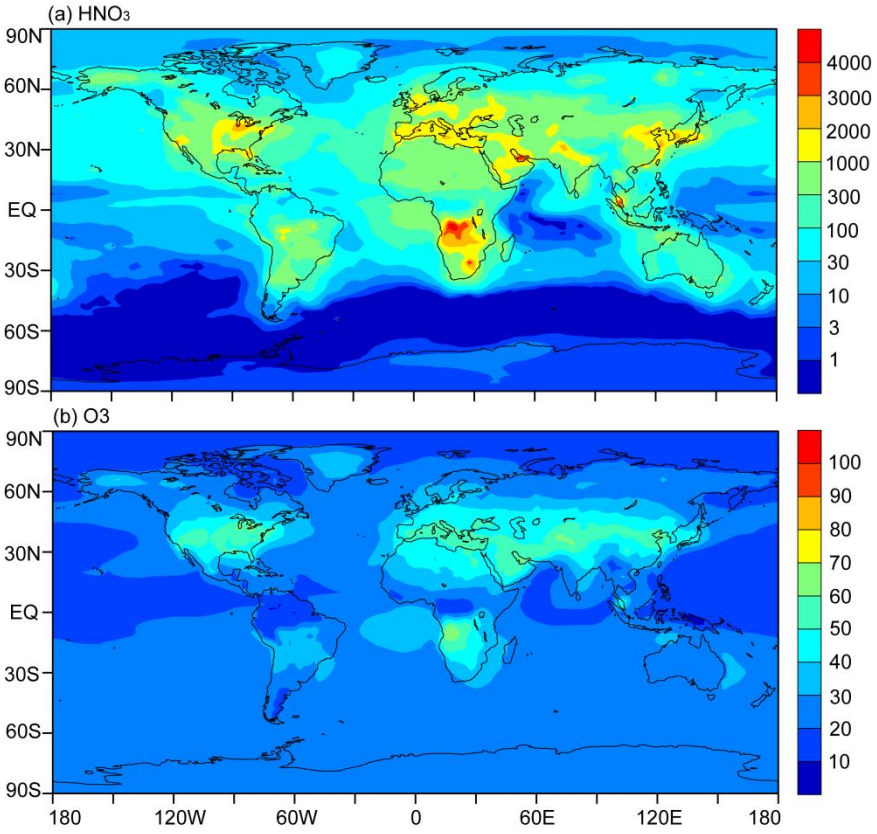

Figure. 3. Simulated global distributions of surface-layer HNO_3 (pptv) and O_3 (ppbv) averaged over June-August, 2005.

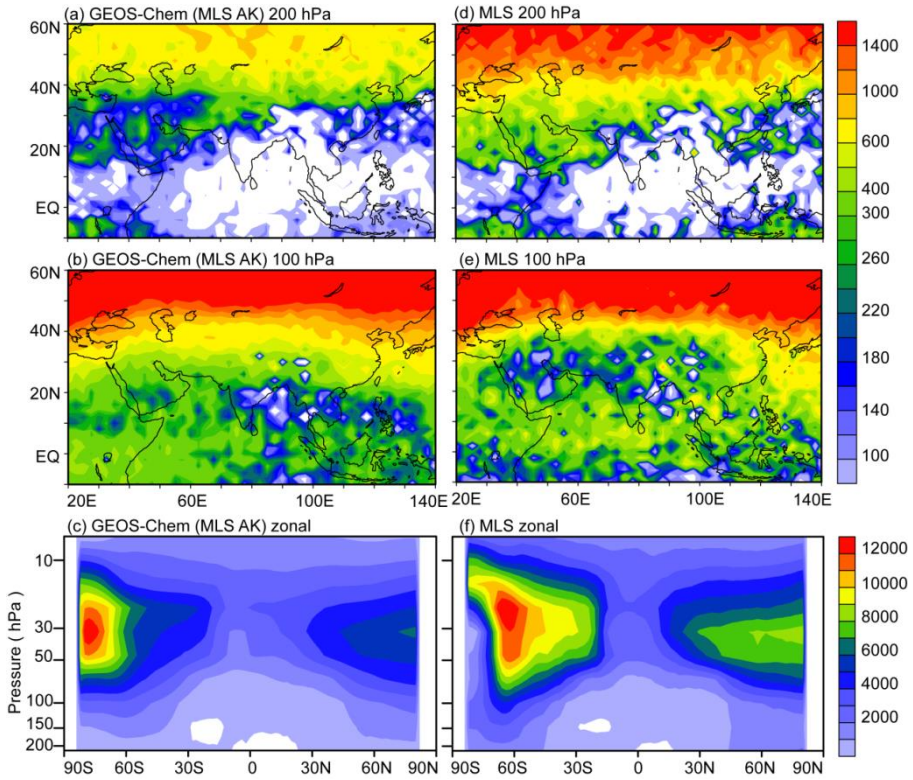

Figure 4. Comparisons of simulated HNO_3 concentrations (pptv) with observations (pptv) from MLS. (a) and (b) are simulated concentrations at 200 hPa and 100 hPa, respectively. (c) is the latitude-altitude cross section of simulated HNO_3 concentrations averaged over 70–105°E. (d)-(f) are the same as (a)-(c), except that (d)-(f) are observations from MLS. The GEOS-Chem HNO_3 simulations are smoothed by the corresponding averaging kernels (AK). White areas indicate lack of data meeting the retrieval quality criteria. All the data are averaged over June-August of 2005.

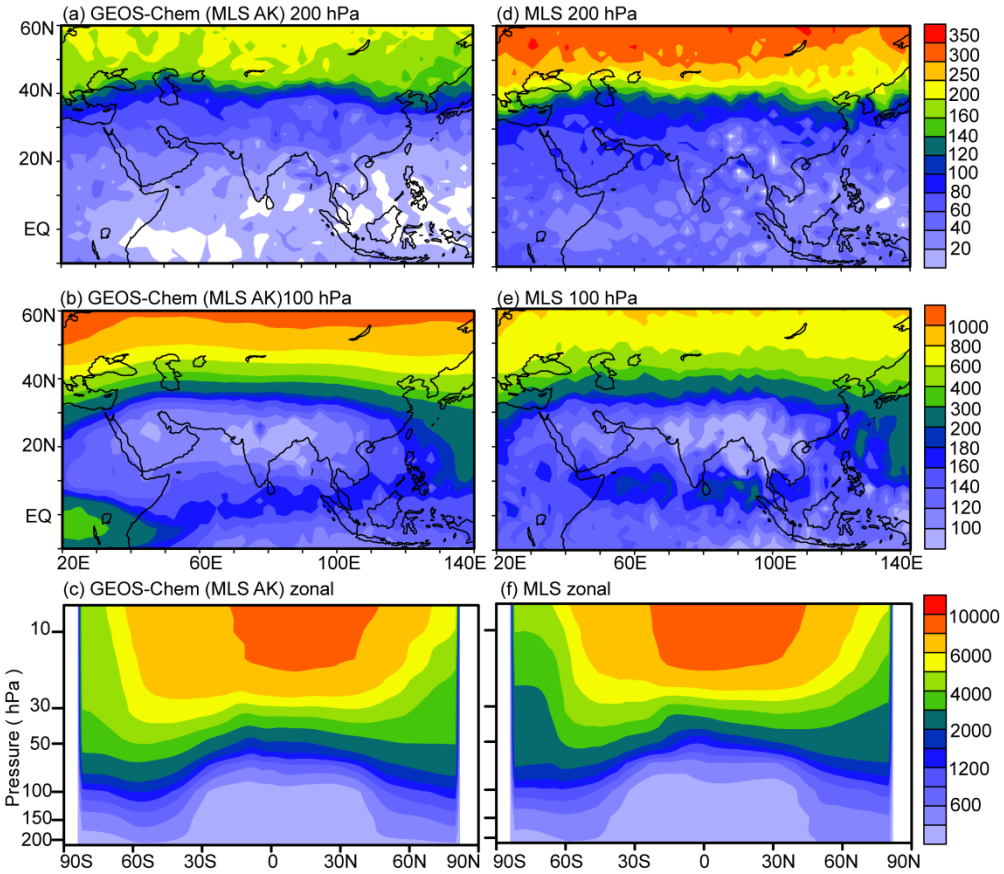

Figure. 5. Comparisons of simulated O_3 concentrations (ppbv) with observations (ppbv) from MLS. (a) and (b) are simulated concentrations at 200 hPa and 100 hPa, respectively. (c) is the latitude-altitude cross section of simulated O_3 concentrations averaged over 70–105°E. (d)-(f) are the same as (a)-(c), except that (d)-(f) are observations from MLS. The GEOS-Chem O_3 simulations are smoothed by the corresponding averaging kernels. White areas indicate lack of data meeting the retrieval quality criteria. All the data are averaged over June-August of 2005.

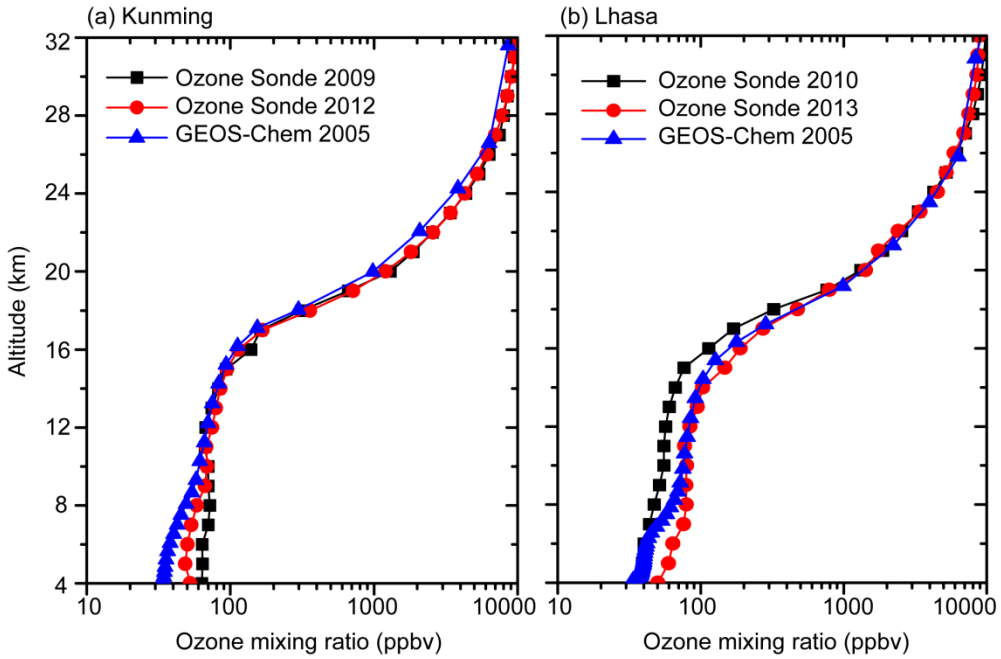

Figure 6. The simulated and observed vertical profiles of monthly mean O_3 mixing ratios at (a) Kunming and (b) Lhasa in August. The model results are from the simulation of year 2005. The observations in Kunming were conducted during August 7–13 (11 profiles of O_3 collected) in 2009 and during August 12–31 in 2012 (daily observations). The observations in Lhasa were conducted during August 22–28 in 2010 (12 profiles of O_3 collected) and during August 4–26 in 2013 (daily observations).

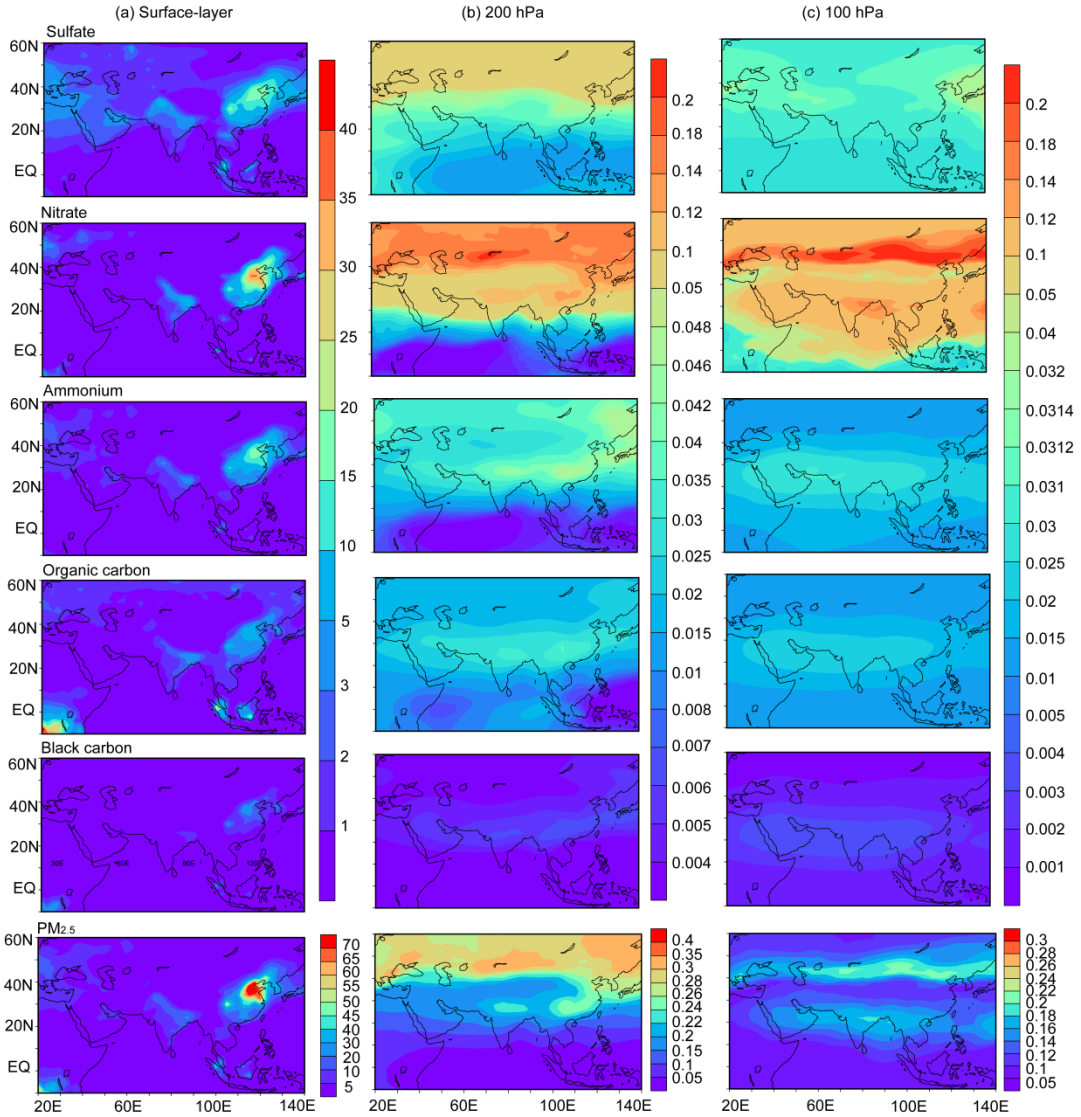

Figure. 7. Simulated seasonal mean concentrations (μg m^{-3}) of sulfate, nitrate, ammonium, organic carbon, black carbon, and $PM_{2.5}$ (defined as the sum of sulfate, nitrate, ammonium, BC, and OC) at (a) the surface layer, (b) 200 hPa, and (c) 100 hPa, during summer (June-August) of year 2005. Note that color bars are different for concentrations at the surface, 200 hPa, and 100 hPa.

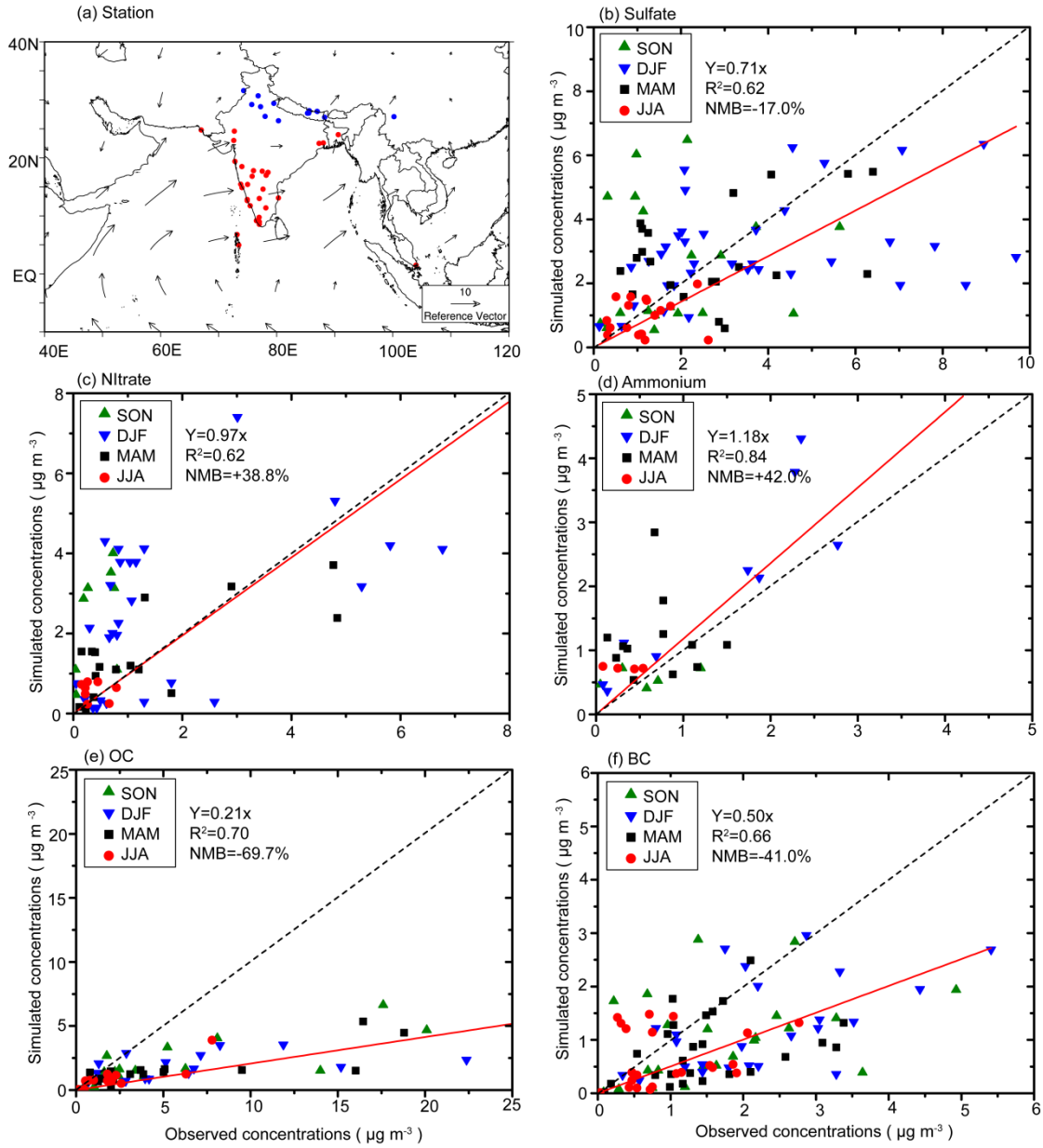

Figure. 8. (a) Locations with measured aerosol concentrations from previous studies over the TP (blue) and SASM (red) region. Also shown are surface winds during summertime. (b)–(f) show the comparisons of simulated seasonal mean concentrations of sulfate, nitrate, ammonium, OC, and BC with measured values, respectively. Also shown in (b)–(f) are the 1:1 line (dashed), linear fit (solid line and equation), correlation coefficient between simulated and measured concentrations (R), and normalized mean bias (NMB) (defined as NMB=$\frac{\sum_{i=1}^{n}(P_i-O_i)}{\sum_{i=1}^{n}O_i}$ ×100%, where P_i and O_i are predicted and observed concentrations at station *i* for each aerosol species).

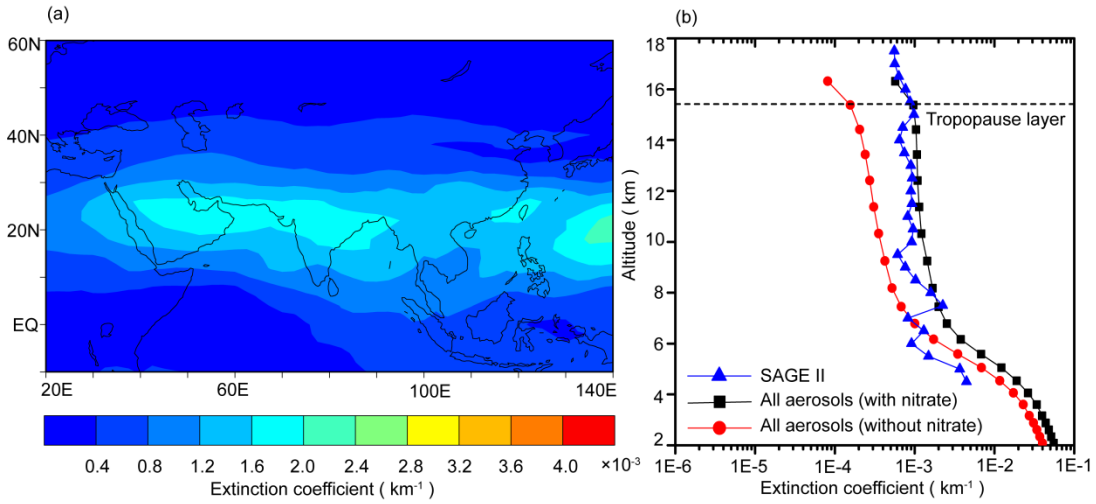

Figure. 9. (a) Monthly mean distribution of aerosol extinction coefficients (km^{-1}) at 100 hPa for July of 2005. (b) Monthly mean vertical distributions of aerosol extinction coefficients (at 525 nm for SAGE II and 550 nm for GEOS-Chem, with the contributions of both anthropogenic and natural aerosols considered) (km^{-1}) averaged over the Asian monsoon anticyclone region (20–120°E, 10–40°N) for July of 2005. The horizontal dashed line represents the tropopause averaged over the Asian monsoon anticyclone region simulated by the GEOS-Chem model.

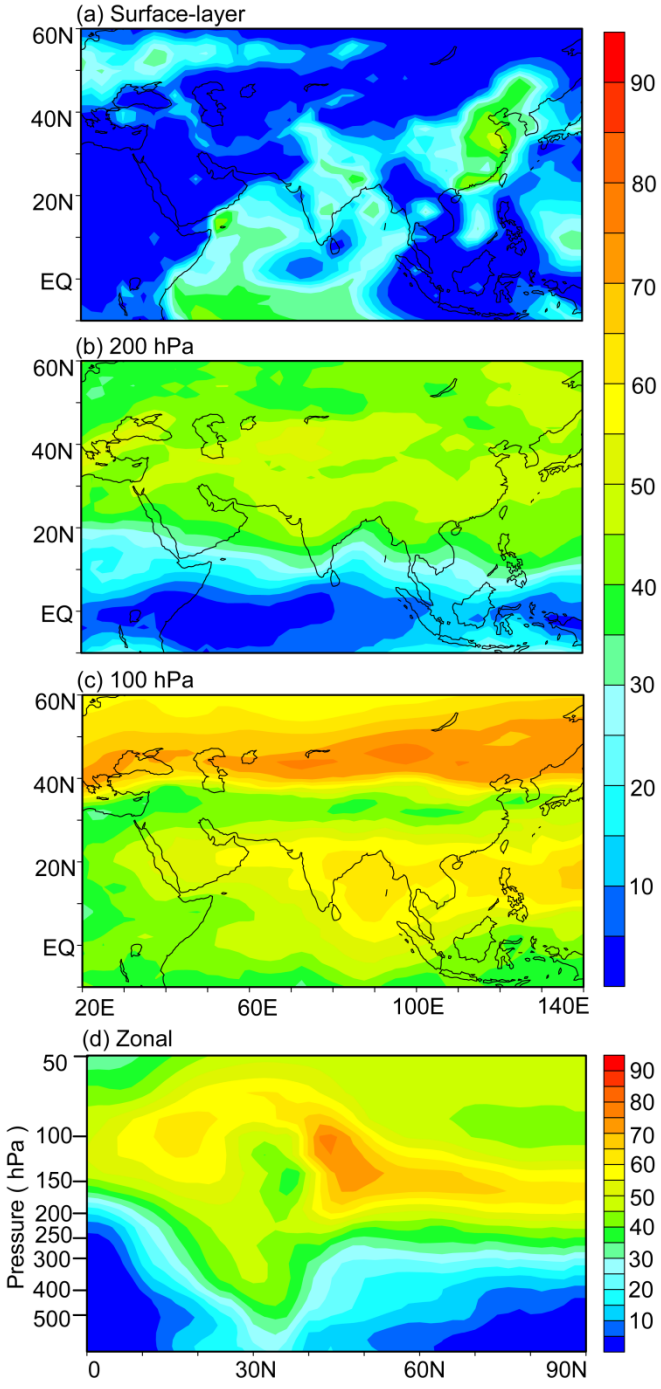

Figure. 10. Simulated contributions of nitrate to $PM_{2.5}$ (C_{NIT}= [NIT]/ [$PM_{2.5}$] ×100%) averaged over summer (June-August) of year 2005 at (a) surface-layer, (b) 200 hPa, and (c) 100 hPa. (d) The latitude-altitude cross section of simulated C_{NIT} (%) averaged over 70–105°E.

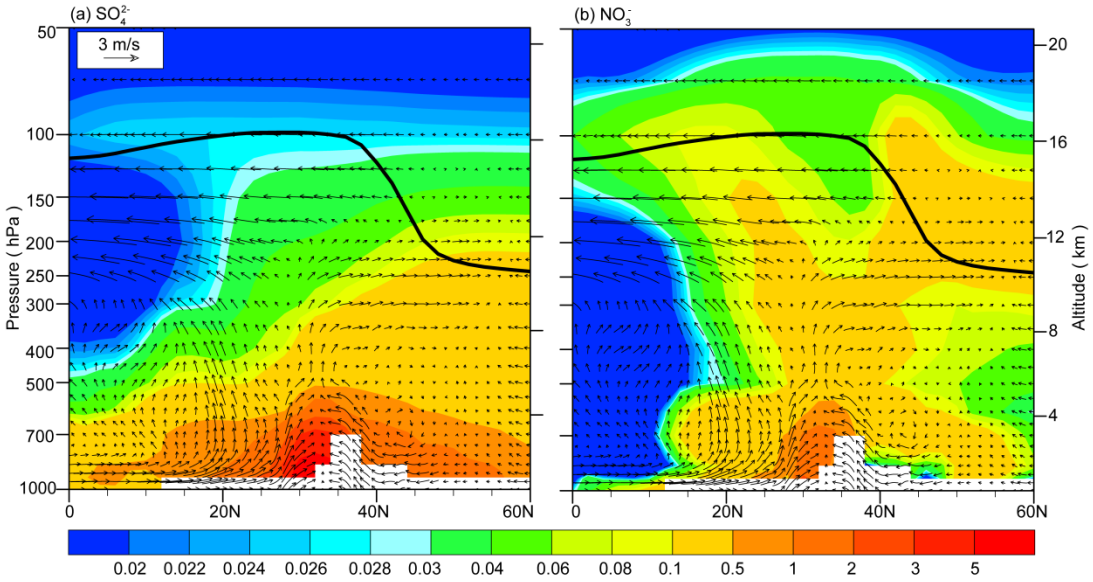

Figure. 11. Latitude-altitude cross sections of simulated concentrations (color shades, μg m^{-3}) of SO_4^{2-} and NO_3^- averaged over 70–105°E in June-August of 2005, together with the wind vectors obtained from the European Centre for Medium-Range Weather Forecasts (ECMWF) ERA-Interim Reanalysis data. The black line is the tropopause simulated by the GEOS-Chem model.

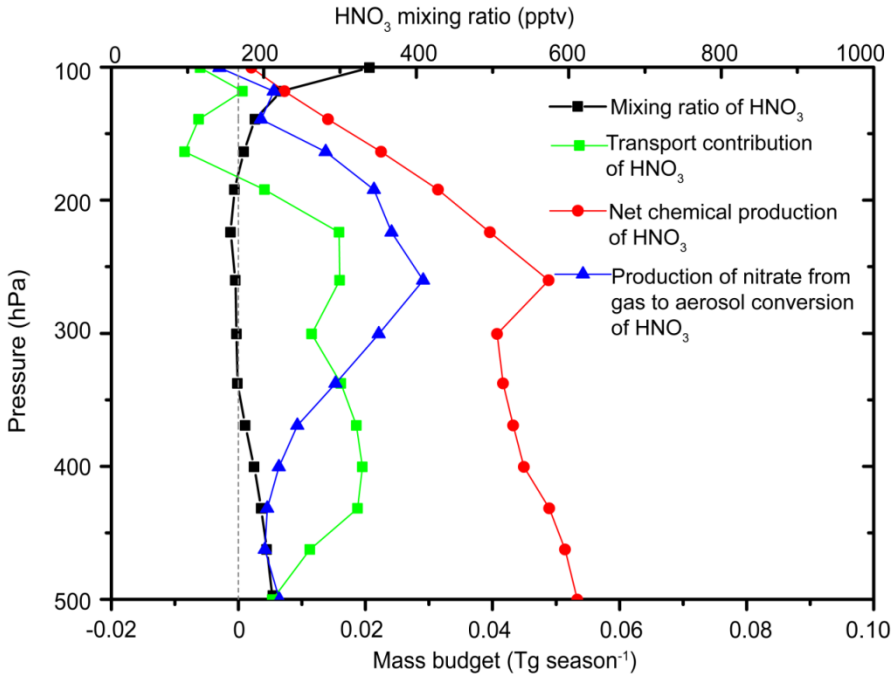

Figure 12. Profiles of the net chemical production of HNO_3 by gas-phase reactions and heterogeneous reactions (red dotted line), the production of nitrate from gas to aerosol conversion of HNO_3 (blue dotted line) and the transport contributions of HNO_3 over the TP/SASM (70–105°E, 10–40°N). Also shown is the average HNO_3 mixing ratios (black dotted line) over the TP/SASM region during summertime of year 2005.

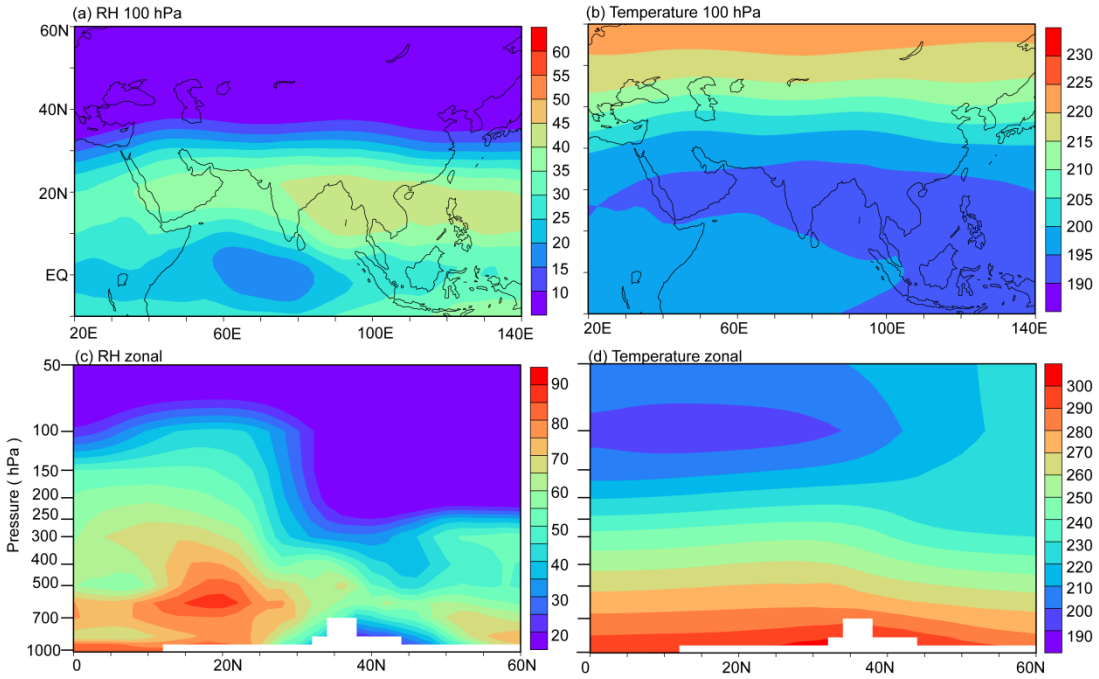

Figure. 13. (a)-(b) Distributions of RH (%) and temperature (K) at 100 hPa. (c)-(d) The latitude-altitude cross sections of RH (%) and temperature (K) averaged over 70–105°E. RH and temperature are from the GEOS5 assimilated meteorological fields, and all the values are the averages over June-August of year 2005.

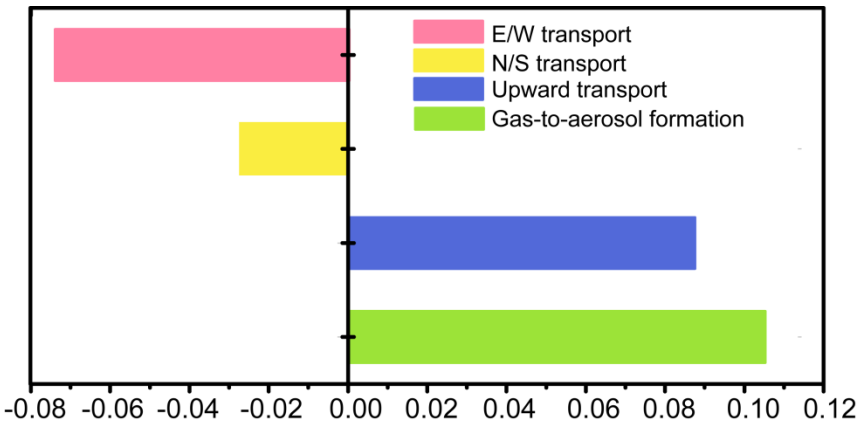

Figure. 14. Mass budget for nitrate aerosol within the selected box of (70–105°E, 10–40°N, 8–16 km). E/W transport indicates net mass flux through the east and west lateral boundaries, N/S transport indicates net mass flux through the north and south lateral boundaries, and upward transport is the net mass flux through the top and bottom sides of the box. The mass flux is positive if it increases nitrate mass within the box. Unit of fluxes is Tg season^{-1}. All the values are the averages over June-August of 2005.